Satellite Observing Systems

Code	SAMOSA-SOA-01	**Edition**	1.0	**Date**	12-02-08
Client	European Space Agency	**Final User**	-		

Development of SAR Altimetry Mode Studies and Applications over Ocean, Coastal Zones and Inland Water

SAMOSA

ESA AO/1-5254/06/I-LG

State of the Art Assessment (WP1) *Version 1.0*

	Name	Signature	Date
Written by	SOS (D Cotton) DMU DNSC (Ole Andersen) NOCS (P Cipollini, C Gommenginger, G Quartly) STARLAB (C Martin, J. Marquez, L Moreno)		
Approved by	Ellis Ash		
Reviewed by	Keith Raney (JHU-APL)		
Authorised by	David Cotton		

DISSEMINATION	COPIES	MEANS
ESA, Jérôme Benveniste	1	Electronic (word and pdf) + Hard Copy
ESA, Jérôme Benveniste	3	Hard Copy
SOS, David Cotton	1	Electronic
NOCS, Paolo Cipollini	1	Electronic
STARLAB, Cristina Martin	1	Electronic
DNSC, Ole Andersen	1	Electronic
DMU, Philippa Berry	1	Electronic
JHU-APL, Keith Raney	1	

SUMMARY OF MODIFICATIONS

Ed.	Date	Chapter	Modification	Author/s
0.99	14/12/07	All	Following comments by KR	DC
1.0	12/02/08	All	Modifications supplied by STARLAB, NOCS, DMU and DNSC. Reviewers comments from KR	CM, CIPO, PB, OA, DC, KR

Table of Contents

1 INTRODUCTION

1.1 Purpose of the Document

This document provides an assessment of the state-of the-art with respect to the data content of SAR mode altimetry, and reviews the observing capabilities of this instrument over water, coastal zones, estuaries, inland water, rivers and lakes. It also assesses the potential for new or further applications of SAR data over those surfaces.

Based on this assessment, recommendations for the rest of the SAMOSA study are provided, in particular on the simulated surface scenarios to generate data with CRYMPS

The authors of this paper will also consider the possibility for presentation at international conferences such as EGU. At the end of the SAMOSA study this paper may be revised and expanded to include any significant new findings.

1.2 Applicable documents

REF.	CODE	TITLE
[AD01]	XCRY-DTEX-EOPS-SW-06-0001	Statement of Work for the Development of SAR Altimetry Mode Studies and Applications over Ocean, Coastal Zones, and Inland Water
[AD02]		Appendix2: Draft Contract

Table 1.1. Applicable Documents

1.3 Reference documents

REF.	CODE	TITLE

Table 1.2. Reference documents

1.4 Abbreviations and acronyms

This section lists the abbreviation and acronyms used in this document.

Abbreviation	Meaning
ASIRAS	ESA Airborne Synthetic Aperture and Interferometric Radar Altimeter System
AT	Along Track
CNES	Centre National d'Etudes Spatiales
CRYMPS	Cryosat Mission and Performance Simulator
CRYOSAT-2	ESA mission to measure cryosphere.
CRYOVEX	Cryosat Validation Experiment
CW	Continuous Wave
DDA	Delay Doppler Altimeter
DEM	Digital Elevation Model
DNSC	Danish National Space Centre, Denmark
DMU	De Montfort University, Leicester, UK
DPM	Detailed Processing Model
D2P	Delay Doppler Phase Monopulse
ERS-1	ESA Remote Sensing satellite launched in 1991, carried EO instruments including a radar altimeter
ERS-2	ESA satellite launched in 1995, (follow on to ERS-1)
ENVISAT	ESA remote sensing satellite launched in 2002, carriying a dual frequency radar altimeter
ESA	European Space Agency
ESRIN	European Space Research Institute
EUMETSAT	European Organisation for the Exploitation of Meteorological Satellites
FFT	Fast Fourier Transform
FM	Frequency Modulated
GEOS	Geostationary Scientific Satellites, operated by ESA, carried an early radar altimeter.
Geosat	US Navy funded altimeter satellite, launched 1985
GFO	Geosat Follow-On, US altimeter satellite, launched 1998
GM	Geodetic Mission
GMES	Global Monitoring for Environment and Security
HW	Hardware
IE	Individual (Radar Altimeter) Echoes
IIP	Instrument Incubator Programme
IFFT	Inverse Fast Fourier Transform
IR	Infra-Red
ISRO	Indian Space Research Institute
JASON	A US-French (dual frequency) altimeter satellite, launched in 2001
JASON-2	A planned US-French altimeter satellite, scheduled for launch in 2008-9
JHU-APL	Johns Hopkins University Applied Physics Laboratory
LRM	Low Resolution Mode
MLE	Maximum Likelihood Estimator
NASA	National Aeronautics and Space Administration
NOAA	National Oceanic and Atmospheric Administration (USA)
NOCS	National Oceanography Centre, Southampton, UK
PRF	Pulse Repetition Frequency
RA-2	Radar Altimeter on ENVISAT
RCMC	Range Cell Migration Correction
RCS	Radar Cross Section
RMS	Root Mean Square
SAR	Synthetic Aperture Radar
SARAL	Satellite with Argos and Altika, planned launch end 2009
Sentinel-3	An ESA satellite planned under the GMES programme. Scheduled for launch ~2012
SIRAL	Synthetic Interferometric Radar ALtimeter
SNR	Signal to Noise Ratio
SOS	Satellite Observing Systems, Co. Ltd., UK
SKYLAB	NASA Space station, operational 1973-74.
SRAL	SAR Radar Altimeter
SSR	Signal to Speckle Ratio
STARLAB	Starlab, Barcelona, Spain
SW	Software
SWH	Significant Wave Height
S-193	Experimental altimeter on SKYLAB
TBD	To Be Defined
TOPEX-Poseidon	A US-French (dual frequency) altimeter satellite, launched in 1992
WITTEX	Walter Inclination Topography and Technology Experiment.

1.5 Document overview

The rest of this document is provided in five sections, as follows

2. Technical overview of SAR altimeter (STARLAB)
3. Review of observing capabilities over open ocean, and recommendations for simulated surface scenarios with respect to sea conditions, sea floor topography and gravity field mapping (NOCS, DNSC)
4. Review of observing capabilities over coastal ocean, and recommendations for simulated surface scenarios (NOCS)
5. Review of observing capabilities over inland water, and recommendations for simulated surface scenarios (DMU)
6. Summary of key findings and recommendations (SOS)

2 TECHNICAL OVERVIEW OF SAR ALTIMETER (STARLAB)

2.1 State of the Art

The first Ku-band pulse limited space-borne radar altimeters date from the 1960´s. They were developed in order to satisfy the needs of the ocean/gravitational science communities. It was in 1973 when the proposal made by *Kaula* [1969] was finally developed; S-193 was flown on board Skylab. After this successful experience, the GEOS C (1975) and SeaSAT-A (1978) missions followed. The Seasat altimeter introduced several design innovations that became standard aspects for all subsequent designs.

GEOSAT (1985), TOPEX/Poseidon (1992), GFO (1998), ERS, ENVISAT and Jason complete the list of satellites that target ocean applications.

CNES included in the TOPEX platform payload the Poseidon altimeter (1992), which was the precursor of the Poseidon series, as hosted on the Jason.

ESA started its involvement at about the same time with its single frequency altimeter, first flown on ERS-1 (1991), and subsequently on ERS-2 (1995).

Later ESA developed a dual frequency Ku and S band altimeter, the RA-2 flown on ENVISAT (2002), which was designed to improve the retrieval of surface elevation and other parameters over a range of surfaces: ocean, inland water, ice and land.

The above mentioned instruments were primarily designed to support investigations into, and generate new knowledge of, key ocean characteristics. The selection of orbit parameters reflected mission priorities, satellite altimeter missions with a repeat orbit period of one year or more were designed to measure the ocean geoid, those with shorter repeat periods, typically 10-35 days, were designed primarily to measure more dynamic ocean features (tides, geostrophic currents, etc.). All altimeters to date have produced waveforms at 10-20 Hz, averaged in processing to yield sea surface topography, and estimates of wind speed and sea state.

Despite the improvements offered by RA-2, conventional pulse limited radar altimeters offer limited practical capability in the near shore region. A solution offering the potential to overcome this limitation is the Delay Doppler radar altimeter [*Raney,* 1998]. While this technique was well supported by theoretical studies, until 1995 there was no numerical proof of it.

The first approach to use phase coherent based instruments appeared in an airborne military system designed, successfully tested in 1962 [*Cutrona* et al., 1962]. After this, the PA-P altimeters on board Venera 15th and 16th (1983) generated phase coherent pulses, allowing digital Doppler processing. Later, *Barbarossa and Picardi* [1990] described a radar altimeter based on Synthetic Aperture Radar (SAR) principles. In addition, *Harlt and Kim* [1990] described the concept of SAR applied to altimetry, considering the interferometric technique, for topography purposes.

As previously stated, in mid 1990 Prof. Keith Raney from the John Hopkins University Applied Physics Laboratory (JHU-APL) proposed the Delay/Doppler radar altimeter concept and in [*Raney*, 1998] provided a detailed description of this new instrument using TOPEX design as a point of reference.

Later, in 1999, through the NASA Instrument Incubator Program (IIP), the JHU-APL tested the Delay/Doppler Phase-Monopulse (D2P). The D2P is a combined airborne synthetic aperture radar and interferometer, which uses the Delay Doppler concept described in [*Raney*, 1998]

At the same time (~1998), ESA started to investigate hardware and software simulation studies for a high-resolution radar altimeter which followed the D2P design [*Raney and Jensen*, 2000] and, based on the Doppler delay concept, combined SAR and interferometry. Subsequently, based on these previous studies, in 2000 Cryosat “phase A” feasibility studies commenced.

Between 2002 and 2005 an experimental campaign of the Synthetic Interferometric Radar Altimeter (SIRAL) designed for operation on Cryosat was carried out using the Airborne SAR/Interferometric Radar Altimeter System (ASIRAS). The campaign provided very promising results. Unfortunately, in

October of 2005 Cryosat was lost during its launch sequence due to a failure of the Eurokot launcher. The current planned launch date for the replacement, Cryosat –2, is between May-November 2009.

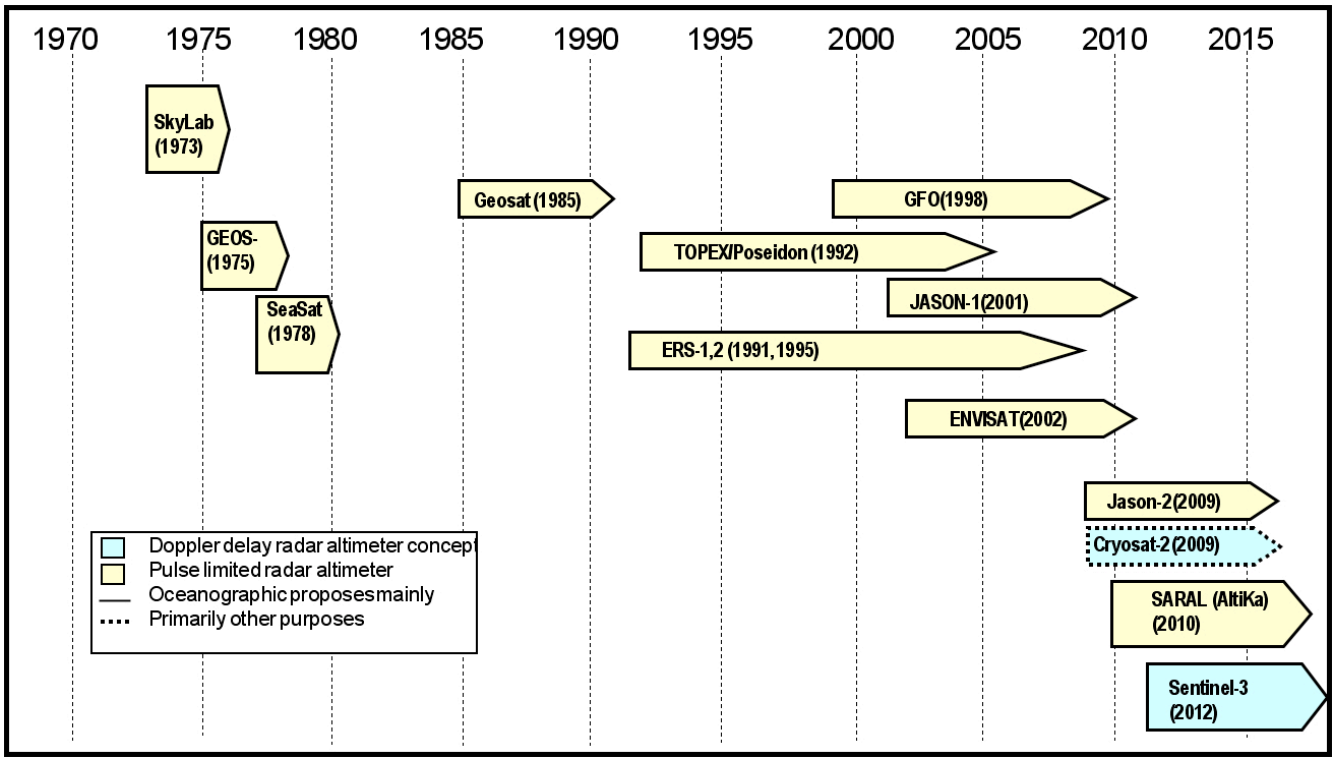

Figure 2-1 Past, current and future altimetry missions

As established and supported through a cooperation agreement between CNES, Eumetsat, NASA and NOAA, Jason-2 is scheduled to take over and continue Topex/Poseidon and Jason-1 mission in 2008. It will carry as its payload the Poseidon-class altimeter named Poseidon-3, the latest of the family carried by the predecessor missions.

Following the failure to launch Cryosat-1 into orbit, Cryosat- 2 will be the first proof of concept for the Delay Doppler altimeter. Its main objective is to reduce uncertainties in the knowledge of sea-ice thickness, and to improve the understanding of the mass balance of the major land ice fields. In addition, the promising capabilities of the sensor for ocean observations open a new door for analyzing the performance of SIRAL over ocean surfaces.

The proposed Water Inclination Topography and Technology Experiment (WITTEX) [*Raney and Porter*, 2000] planned a application of this technical development to ocean measurements, with an approach that would meet nearly all the requirements identified by the user community for oceanographic altimetry. A constellation of three Doppler Delay Altimeter (DDA) satellites was proposed, with the satellites to be placed in the same orbit plane. However, funding was not approved for WITTEX.

“Satellite with ARgos and ALtiKa” (SARAL 2009) is a co-operative altimetry technology mission between the Indian Space Research Organization (ISRO) and CNES. The SARAL mission is considered to be complementary to the Jason-2 mission and, with a planned launch date towards the end of 2009 will help to fill the gap between Envisat and the Sentinel-3 mission of the European GMES program. The payload includes an altimeter in Ka band, AltiKa, which will be the first space-borne altimeter to operate at Ka-band.

ESA has also proposed the inclusion, in its Global Monitoring for Environment and Security (GMES) programme, of a SAR based Radar altimeter on the Sentinel-3 mission. The SAR Radar Altimeter **(**SRAL**)** builds on the strong heritage of the instrument techniques implemented for the Poseidon-3 altimeter and for SIRAL (SAR Interferometer Radar Altimeter) on CryoSat-2. Initial planning identifies 2012 as the earliest possible date for the launch.

2.2 Brief Review of Radar Principles

Before describing the basics of conventional altimetry and SAR altimetry, the principles of a radar system shall be reviewed. In this chapter, a brief description of the functionality of a radar system is provided. To describe the radar equation two different observation geometries will be considered: a general radar observation, and a satellite or air borne geometry. Specifically, the transmission, redirection and reception of the radar signals are analyzed.

Figure 2-2 illustrates a general radar observation geometry with a transmitting antenna, a target, and a receiving antenna.

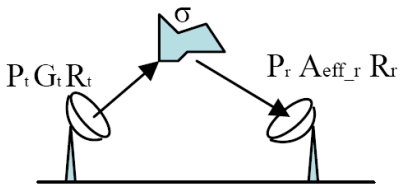

Figure 2-2: General Radar Geometry

Using the naming convention as in the previous figure, the radar equation for the power received is given by:

$$P_r = \left(\frac{P_t}{4\pi R_t^2}\right)\left(G_t\right)\left(\sigma\right)\left(\frac{1}{4\pi R_r^2}\right)\left(A_{eff\_r}\right). \qquad (1)$$

The variables of the equation are:

P_t - power transmitted [watts]

P_r - power received [watts]

R_t - range distance between scattering point and transmitting antenna [m]

R_r - range distance between scattering point and receiving antenna [m]

G_t - gain of transmitting antenna [dimensionless]

σ - radar cross section (RCS) of the scattering surface [m^2]

A_{eff_r} - effective aperture of receiving antenna [m^2]

Five different factors can be identified in the radar equation. All can be related to physical terms as described below:

$\left(\frac{P_t}{4\pi R_t^2}\right)$ - is the power density of a spherical wave carrying power P_t at a distance R_t from the source.

$\left(G_t\right)$ - gain is related to directivity through $G(\theta,\phi) = \eta_l D(\theta,\phi)$. The directivity *D* is the ratio between the power density emitted towards a particular direction, at distance R, versus the power density that the same antenna would emit isotropically at the same distance. η_l is the antenna efficiency which in case of lossless antennas is equal to 1 (thus for such antennas directivity and gain are equivalent).

$\left(\sigma\right)$ - The RCS describes the ability of the scattering surface to redirect the power from the transmitting antenna towards the receiving antenna. It is usually related to the area under observation by: $\sigma = \sigma_0 A_\sigma$, with σ_0 being the normalized RCS, and A_σ the area of the resolved footprint.

$\left(\frac{1}{4\pi R_r^2}\right)$ - From scattering theory, this term scales the scattered power by the area of a sphere through which it flows, with the radius equal to the distance from the scatter to the receiving antenna.

$\left(A_{eff\_r}\right)$ - is the effective aperture of the receiving antenna, which relates to the antenna gain by:

$A_{eff} = \frac{G\lambda^2}{4\pi}$.

The general radar observation geometry is now modified to represent an airborne or satellite geometry more representative of an altimetric observation.

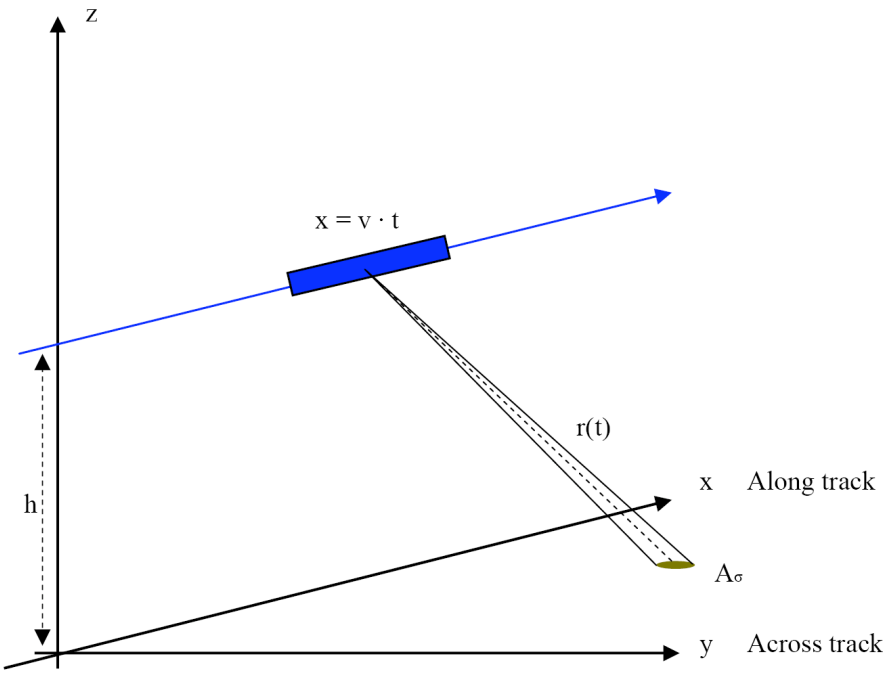

Figure 2-3 Air borne or satellite radar observation geometry

Figure 2-3 shows a moving platform observing a small area over the surface. For convenience, the along track direction, corresponding to the flight track, is usually assumed to be define the “x” axis. For simplification, our airplane or satellite will move at velocity *v* = *(v_x, 0, 0)* at distance *h* from the (x, y) plane which corresponds to the observed surface. The across track dimension corresponds to the direction perpendicular to the along track, which for simplicity in this chapter will be the observation direction. Further observation geometries have been considered in radar, like squint angle geometries, but for the purpose of this section let us assume a lateral observation or across track observation.

The antenna beam will define an area over the plane (x, y) known as the area under observation of our sensor, previously referred to as the area of the resolved footprint A_σ.

The receiving and transmitting antennas, for simplicity, are considered to be the same. Therefore, the transmitting distance and receiving distance are also equal.

For such a system, the radar equation simplifies to:

$$P_r = \frac{P_t G^2 \sigma_0 A_\sigma \lambda^2}{(4\pi)^3 R^4}. \qquad (2)$$

2.3 Radar Altimetry

The previous section described the basic concepts behind radar altimetry. This chapter introduces the concept of the conventional radar altimetry as necessary to support the description of the SAR altimetry mode, provided in section 2.4. The different measurements, observation geometries, and radar altimetry system functionalities are described below.

2.3.1 Radar Altimetry Concept

In the introduction, radar altimetry has been described as the measurement of the time t_d of a radio signal to travel from the emitting instrument, reach a target surface, and return/scatter back. Altimetric measurements allow the detection of physical parameters listed below:

- **Range:** distance from the satellite's centre mass to the sea surface $t_d = \frac{2R}{c}$ (c = speed of light) (needs atmospheric, sea-state, etc., corrections)
- **Significant wave height (SWH):** "*is the average height (through to crest) of the 1/3 largest waves*". Essentially, this is 4 times the standard deviation of the surface. Measurable from the slope of the leading edge of the waveforms.
- **Wind Speed**: The (non-directional) wind speed at the ocean surface (the standard reference height is in fact 10m), estimated through its relation to the small (cm) scale ocean surface roughness which in turn is related to the surface backscatter.

Figure 2-4 provides an example of conventional pulse limited altimetry geometry. Radar altimetry measurements can be achieved using different emission types: mono pulse or burst of pulses, continuous emission, dual frequency emissions, etc. For this technical note, and in order to introduce the SAR Altimetry mode presented in the following chapter, this section only describes a single frequency system emitting a burst of pulses.

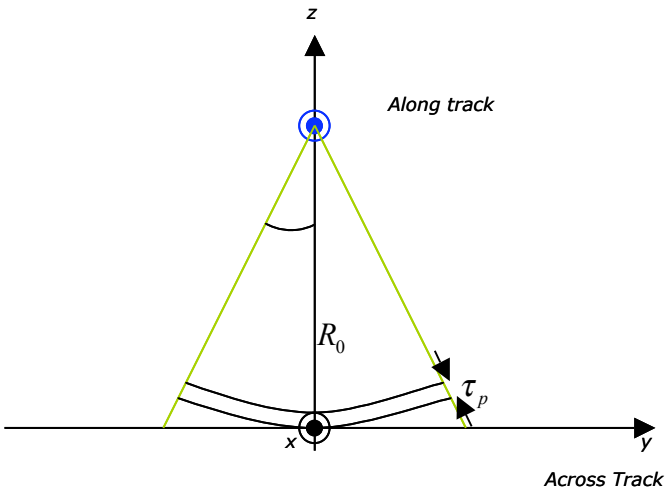

Figure 2-4 Conventional Altimetry observation geometry. Pulse limited. τ_p = pulse length

Before an analysis of the echo return from a burst of pulses it is convenient to introduce the echo return of a single emitted pulse.

Figure 2-5 a) shows the propagation of a single pulse along the beam of the antenna in the (z, y) plane, corresponding to a flat surface. The curved lines represent the pulse propagating and the temporal width between curves is constant and equal to τ_p, the duration of the pulse length. A different

visualization of the propagation (looking down on the scattering surface from the instrument position) is provided in Figure 2-5 b). At the time the pulse reaches the observed surface, and until all the width of the pulse is in contact with the surface, the area illuminated by the emitted pulse will be defined by a circle, as the pulse propagates the circle transforms into rings of equal area [*Fu and Cazenave,* 2001].

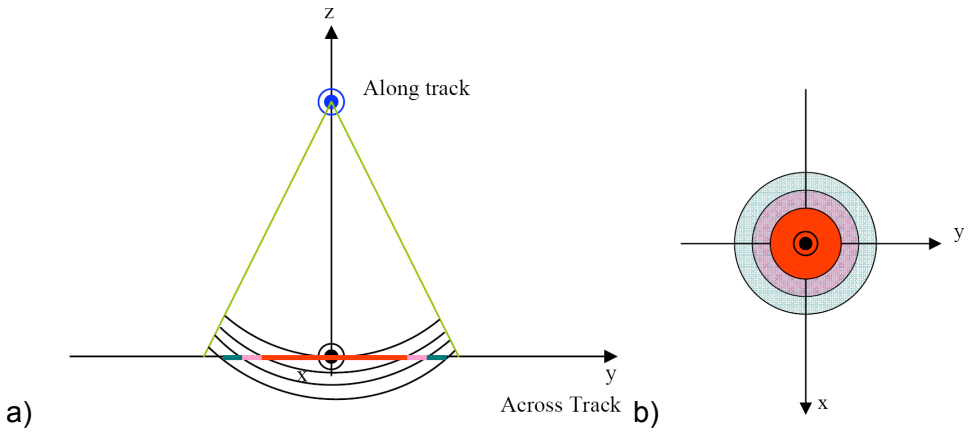

Figure 2-5 Mono Frequency – mono pulse system; a) Measurement geometry, b) surface footprint

With no further information, Figure 2-5 b) could lead to the conclusion that all the scattering contributions from the points within the same circle or rings would be indistinguishable, given that they will be received simultaneously. However, this only applies if sensor and target are static, which is not the case in our geometry. Due to the sensor movement, airborne or satellite altimetry is also affected by the Doppler effect, which allows some further discrimination, as discussed in more detail later.

2.3.2 Radar Altimetry Burst of Pulses

In section 2.3.1 we introduced the concept of bursts of pulses. Conventional altimeters usually emit a burst of pulses which observe almost the same footprint. This will result into more looks of the same footprint, thus will reduce the speckle noise effect. Pulse to pulse coherence is neither necessary nor desirable in conventional altimetry because incoherent, de-correlated averaging is needed for speckle reduction.

2.3.3 De-ramp Technique

In satellite or airborne radar observations, at any given time the sensor receives contributions from all points within one physical pulse length.

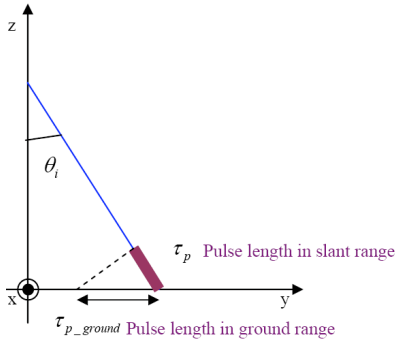

Figure 2-6 Pulse resolution

The size of the scattered area in the slant range direction contributing to the echo at any given time can be measured as:

$$\delta_{SR} = \frac{c\tau_p}{2}. \qquad (3)$$

Therefore, the emitted pulse length defines the resolution of the observation. Thus, pulses of short duration are needed to obtain high precision. To overcome the constraint of short duration pulses altimetry measurements benefit from the properties of chirp signals. Very short pulses with very high transmitted power are achieved through injection of short pulses into a dispersive delay line, resulting into a frequency modulated (FM) signal known as chirp. In chirp systems the resolution is determined by the signal bandwith. Thus, the resolution is now longer determined by the pulse width, but rather by the chirp frequency range.

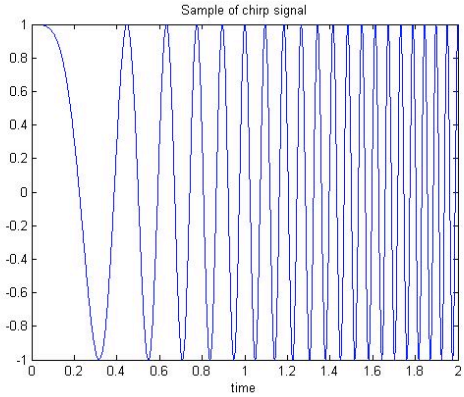

Figure 2-7 Chirp signal sample

Chirp signals can be mathematically written as:

$$s(t) = u(t) \cdot e^{-i2\pi f(t)t - \varphi_0}. \qquad (4)$$

With $u(t)$ a rectangular function with length τ_p (pulse duration); $f(t) = \frac{s}{2}t + f_c$ the frequency of the chirp signal which is time dependant; f_c the central frequency; $s = \frac{B_p}{\tau}$ the chirp slope dependent on the pulse chirp bandwidth and the pulse duration. For simplicity let us assume ϕ_0 equal to zero here. Schematically the frequency-time relationship of chirp signals is:

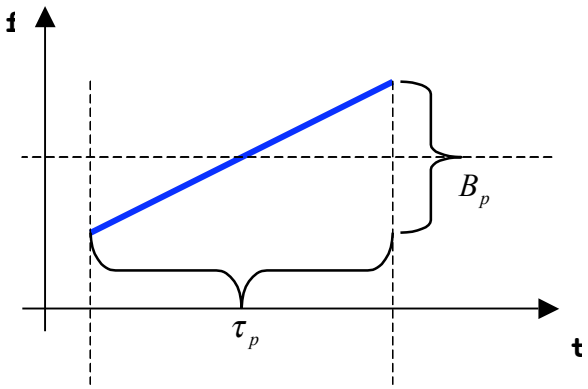

Figure 2-8 Frequency – time relation of a Chirp signal

It is difficult in practice to generate short pulses with sufficient power to ensure an adequate signal-to-noise ratio (SNR). As solution to this problem compression techniques are applied to obtain equivalent information from longer emitted pulses. To resolve this problem, altimeters use the deramp technique.

Deramp was introduced by *MacArthur et al.*[1987] in the design for the SEASAT altimeter. It is also known in the wider radar world as the “Stretch” technique, originally introduced by *Caputi* [1971]. The full deramp method requires two distinct operations: a time domain multiplication of the backscatter

signal by a delayed replica of the transmitted linear FM waveform (deramp), which generates a continuous wave (CW) signal (see figure 2-10), and an Inverse Fast Fourier Transform (IFFT) of this CW.

Figure 2-9 shows a schematic representation of a transmitted chirp signal, its received backscattered echo, and the deramping chirp. t_d is the deramp time delay, which if it is suitable is set to match the arrival time of the received echo which should be equal to the two way travel time from the altimeter to the mean sea level (t_0). If this does not occur and t_d is set earlier or later than t_0 then the frequency of the resulting CW will be affected by a factor $\Delta f = s\Delta t$ where s is the original chirp slope, as presented below.

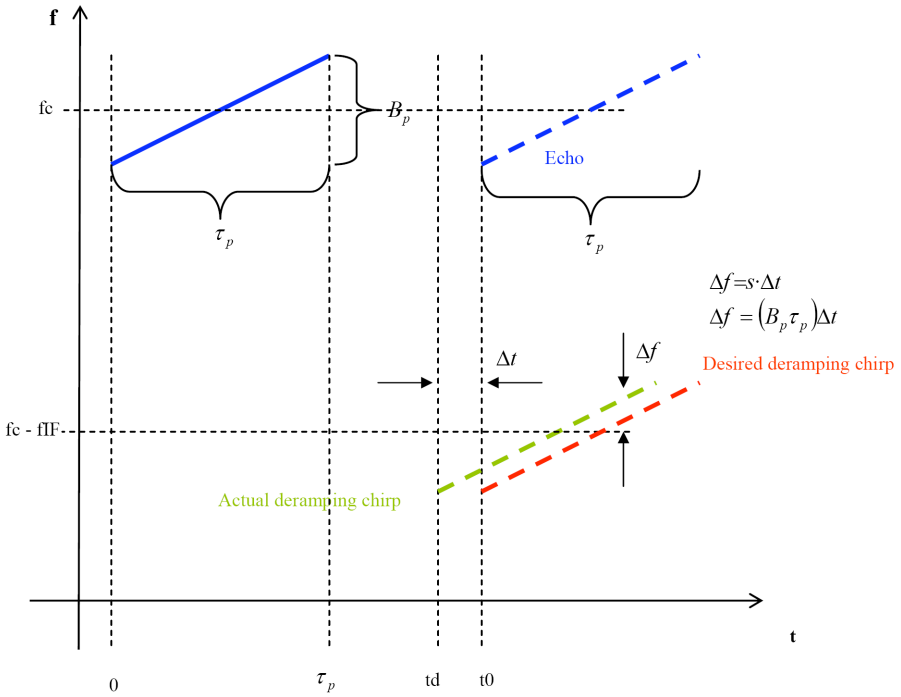

Figure 2-9: Schematic representation of the transmission and reflection of a Chirp signal. [*Chelton et al.*,, 1989] figure 6 including transmission phase.

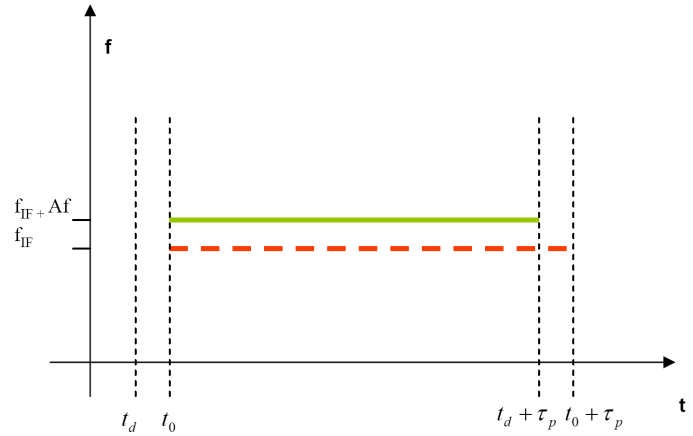

Figure2-10: De-ramp result. Example from [*Chelton et al.*,, 1989] Figure 6.The purpose of this approach is to measure the frequency difference, Δf , which is proportional to the range.

A key outcome of the deramp method is the fact that each CW frequency is linearly related to the travel time, and hence the radar range, of each individual backscattering element relative to the $\Delta t_d = t_0 - t_d$ chosen for the deramp replica.

For each individual emitted pulse a set of echoes from different scatterers will be received. The number of echoes received per pulse emitted will be dependent on the reception window, usually specified so that echoes from the previous emitted pulse are not received.

Bearing this in mind, and considering figures 2-9, 2-10, it can be seen that each emitted chirp will result in an echo whose shape is defined by the backscatter contributions of the footprints on the sea surface illuminated by the transmitted pulse (see Figure 2-5). Therefore, the echo received will be a set of chirp signals received at different delay times. The receiver will deramp each individual echo contribution, thus the final result can be schematically represented in the following figure:

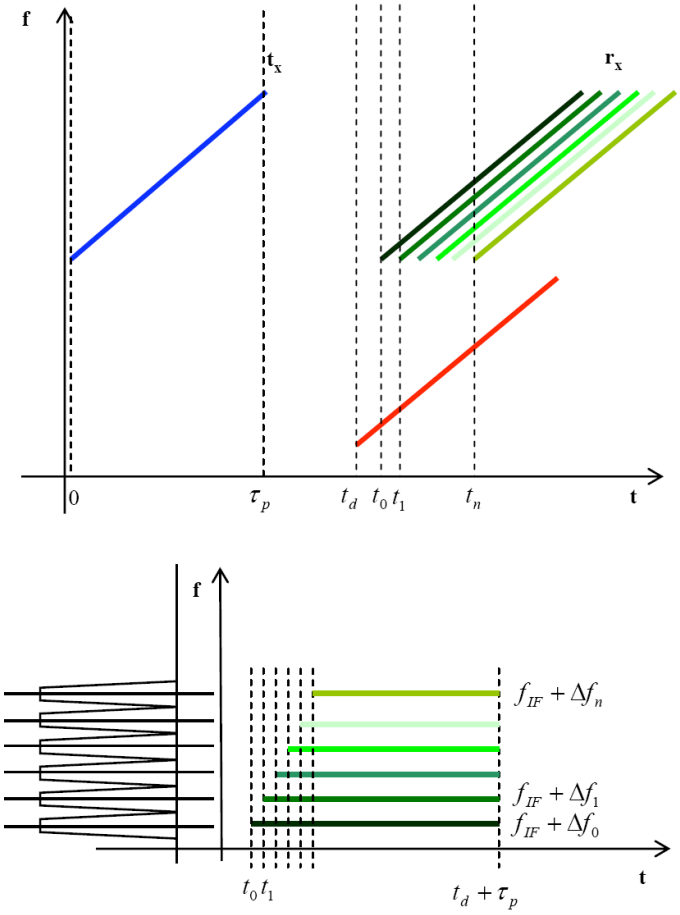

Figure 2-11: Deramp technique applied to a received echo

The second of the operations in the full deramp process is an IFFT which compresses all the CW wave signals to a position that is proportional to their frequency. The resolution achieved is then inversely proportional to the length of the IFFT. Considering that before the IFFT and after the deramp we have very low bandwidth signals it can be seen that it is possible to achieve fine resolutions with this methodology.

2.3.4 Conventional Altimetry Block Diagram

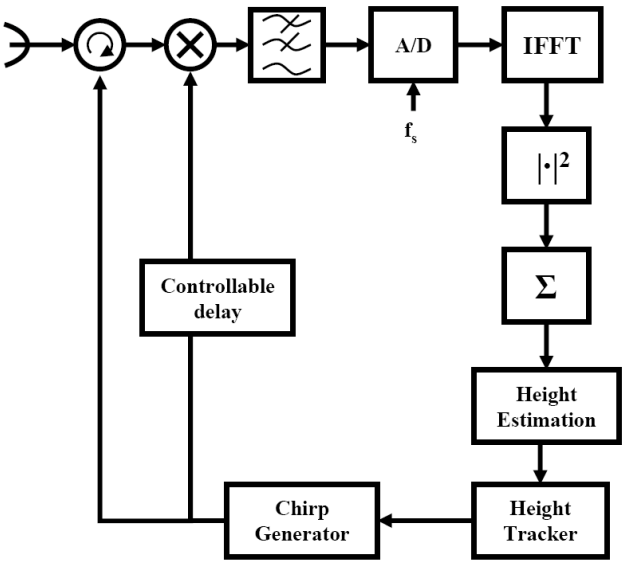

Figure 2-12 High Level Conventional Altimetry Block diagram

Figure 2-12 shows a high-level conventional altimeter block diagram. This view is restricted to represent only the essential components on the receiver side. The first blocks (multiplier and IFFT) have been already described in the previous sections.

A burst of chirp pulses is transmitted and the returned echoes are deramped and subjected to an IFFT. After the echoes are transformed to power echoes the power echoes from the different pulses transmitted are incoherently averaged and the final result is normalized for height estimation. Estimation and height tracker have not been analyzed in this document yet. Both blocks are dependent on the final normalized power echo, which is described in the following section.

2.3.5 Return Mean Echo over Ocean

In this section a generalized rough surface response is introduced to allow a better understanding of functions within the altimeter block diagram, specifically the height estimation and height tracker.

Previous studies have demonstrated that the impulse response of an ocean surface can be represented as follows [*Brown*, 1977], [*Hayne*, 1980], [*Chelton et al*., 1989].

Figure 2-13 illustrates the power received by a satellite altimeter (after incoherent averaging). The two-way travel time for the leading pulse edge to propagate from the altimeter to the surface crest is . For a calm sea surface, the power rise time is the compressed effective pulse duration τ_p. For a rough sea surface with significant wave height[1] (SWH) $H_{1/3}$, this rise time increases by (*2c-1*) x $H_{1/3}$ [*Chelton et al*., 1989]. The half power point defines t_0 which corresponds to the two-way travel time to the mean sea level (MSL). In addition, the area under the curve is proportional to the nadir incidence NRCS σ^0 .

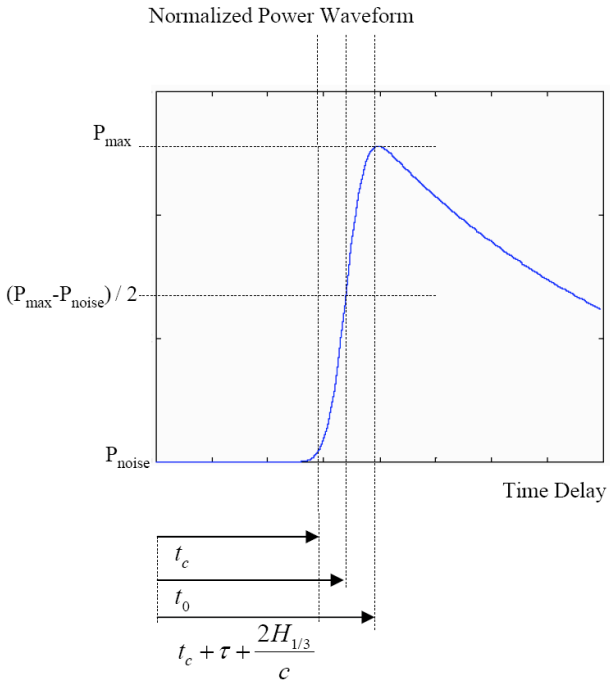

Figure2-13: Power received by the altimeter after incoherent averaging.

Figure 2-13 clearly shows that the estimates for the delay (range related), the SWH and the surface wind speed (dependent on the NRCS) can be derived from the impulse response. *[Brown*, 1977] and then [*Hayne*, 1980] introduced the mathematical expression of the average impulse response of a rough surface and detailed the specific case of ocean surfaces. Through the comparison of the theoretical waveform and the measured waveform all the parameters mentioned above (range, SWH, wind speed) can be estimated. Comparison techniques are out of the scope of this deliverable and will not be detailed in this document.

2.4 SAR Altimetry

SAR altimetry was first described as Delay/Doppler radar altimetry by *Raney,* [1998]. In this section, the terms Delay/Doppler radar altimetry and SAR altimetry are used interchangeably. The key innovation of SAR altimetry is the addition of along track processing for increased resolution and multi-look processing. This technique requires echo delay compensation, analogous to range cell migration correction in conventional but unfocused SAR [*Raney,* 1994]. Due to this innovation, spatial resolution is increased in the along-track dimension and Delay/Doppler mapping is provided. In turn, this allows for accumulation of more statistically independent looks for each scattering area, leading to better speckle reduction and altimetric performance.

This section describes SAR altimetry mode, SAR geometry, the Delay/Doppler concept, and the performance of SAR Altimetry versus conventional altimetry will be discussed.

2.4.1 Doppler Effect in Radar Altimetry

The relative motion between the observing sensor and the target, in radar observations results in an effect known as the Doppler effect.

Assuming a static observer and a moving target, Figure 2-14 displays the emission of two pulses at a time distance T_0. The time for the fist pulse to reach the moving target is t_1, the time for the second emitted pulse to reach the target is t_2. Due to the target motion, the first pulse will reach the target at a distance R_1, but the second emitted pulse will reach the target at a larger distance R_2.

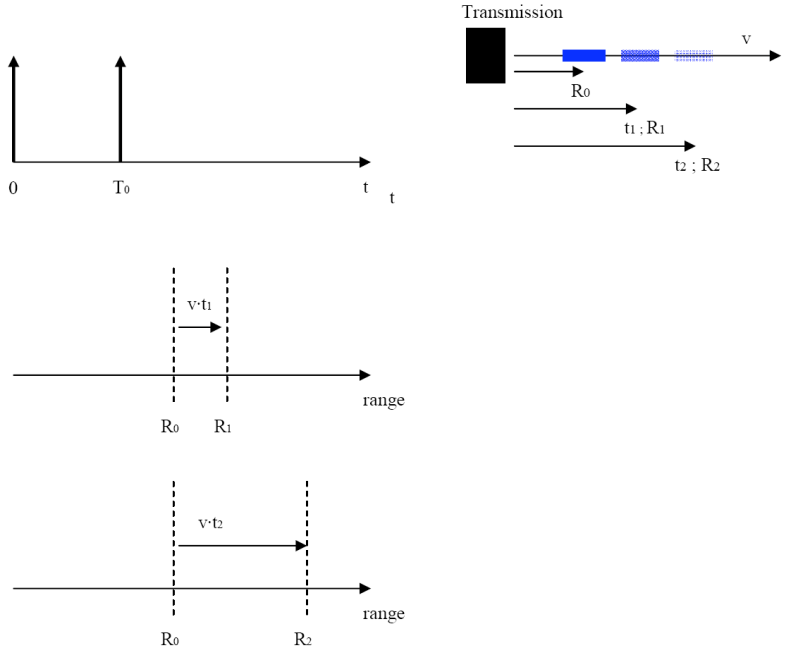

Figure 2-14 Doppler effect of a moving target

The difference in reception times of the two echoes can be related to frequency changes by:

$$f_r = \frac{1}{t_2 - t_1} = \frac{(c-v)}{(c+v)} \cdot \frac{1}{T} = \frac{(c-v)}{(c+v)} f_0 . \qquad (5)$$

We refer to the difference of the previous frequency and the original emission rate ($f_0 = \frac{1}{T_0}$) as the Doppler frequency.

$$f_D = f_r - f_0 \approx -2\frac{v f_0}{c} . \qquad (6)$$

for $c >> v$ (non-relativistic)

From the above, and considering the observation geometries in Figure 2-4 and Figure 2-5 , it can be send that all the contributions from the same ring will not have the same Doppler frequency. Therefore, the footprint view in Figure 2-5 b) will be modified as presented in Figure 2-15, below.

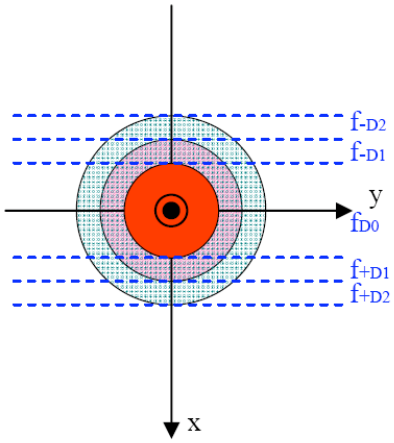

Figure 2-15 Doppler frequency map

Considering the Doppler affect, the two contributions from the same ring in the along track (x-) direction (in front of, and behind nadir) will be distinguishable. On the contrary, the contributions from

the same ring in the across track (y-) direction (left and right of nadir) will be received simultaneously and will not be separable.

2.4.2 SAR Observation Geometry

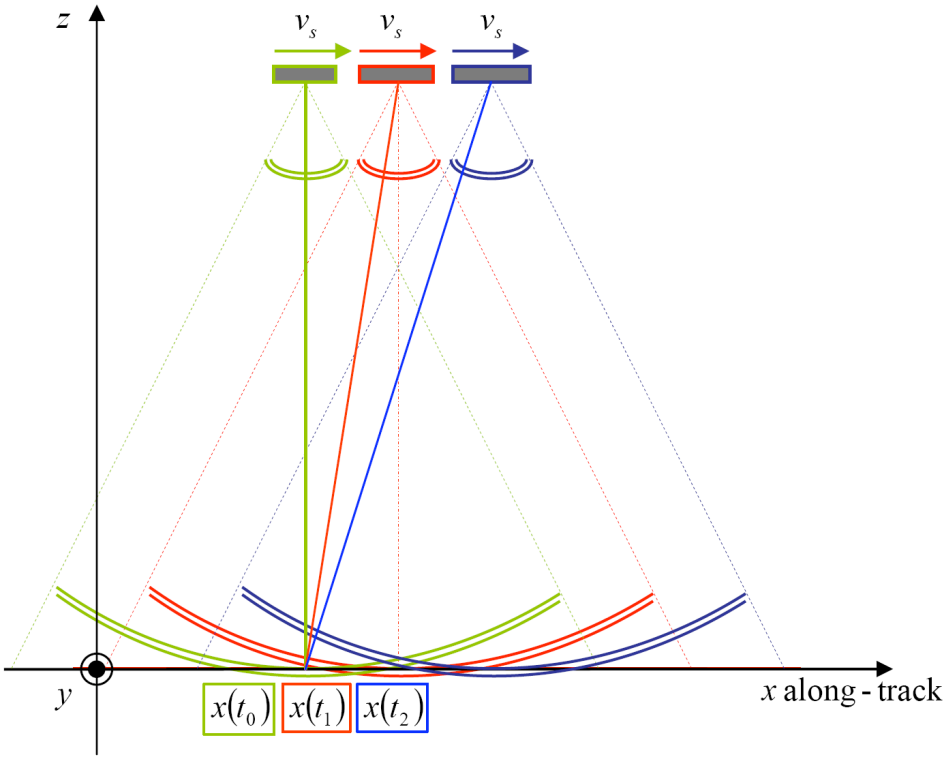

Figure 2-16: SAR Observation geometry of a scattering point

SAR altimetry processes the data such that they could be seen as having been acquired from a synthetic aperture antenna. Thus, the contribution from a scattering point will be distinguishable as the airborne or satellite platform moves. Figure 2-16 shows the observation geometry of a scattering point in SAR altimetry mode. In effect, SAR altimetry spotlights each resolved along-track cell as the radar passes overhead. Differently to conventional altimeters, SAR altimeters use most of the power received, in fact in conventional altimetry the power contribution of the scattering points adjacent to the one of interest is lost.

2.4.3 SAR Altimetry Concept

Delay/Doppler radar altimetry benefits from the conventional pulse compression in the range dimension as explained in section 2.3.4. Additionally, SAR altimetry introduces along-track processing for azimuth mapping. The main requirement for the use of the SAR processing in altimetry is the coherency within each burst of pulses [*Raney,* 1998], which differs from conventional altimetry as described in section 2.3.3. Thus the PRF must be larger than the Doppler bandwidth of the spectrum of the along-track antenna beam-width. The basic processing steps of the SAR altimeter are depicted in Figure 2-17. Note that this is a simplified block diagram intended for conceptual algorithm representation, i.e. it is not Hardware (HW)/ Software (SW) optimized.

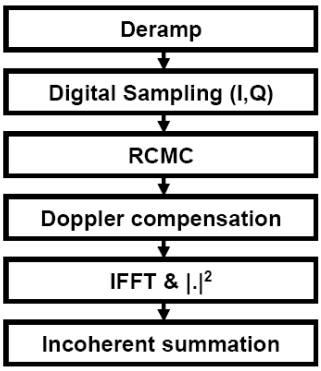

Figure 2-17: Basic steps of the SAR altimeter processing

The Delay/Doppler altimeter, just as with a conventional altimeter, uses full deramp and IFFT compression in the range dimension. The range signal, a frequency modulated pulse or chirp, is multiplied by a delayed replica of the transmitted signal, low pass filtered and compressed by means of an FFT. The range-compressed echoes are stored in the "slow-time" or along-track dimension resulting in a 2D data matrix. In addition, an along-track FFT is applied to the data in order to map the Doppler frequency of each echo. The Doppler frequency is related to the relative position of the scatterer with respect to the movement of the satellite. The known position of the scatter delay time correction is applied to each Doppler bin. Next to the compensation, the range position (i.e. delay time) of each scatterer over its entire illumination history is equal to its minimum range; this process is applied burst-by-burst. The Doppler shift is performed in order to place the information of each scatterer, distributed in different bursts at different Doppler bins, in the same Doppler bin. As described this process facilitates the average waveform retrieval. Using SAR altimetry the contribution of adjacent scatters will be effectively minimized, and the desired scatterer contribution maximized for each computed waveform (see section 2.4.3.5). Note that the influence of adjacent targets in the final waveform depends on impulse response of the system.

2.4.3.1 Range Resolution

Delay/Doppler radar altimeters use the same full deramp and IFFT pulse compression scheme, as conventional incoherent radar altimeters; see section 2.3.4.

2.4.3.2 Doppler Position Mapping

The Doppler position mapping refers to the Fourier transform of the 2D data matrix in along-track direction. Subsequent to this operation, the information of the different scatterers is redistributed depending on their relative position with respect to that of the satellite.

The Doppler spectrum has a geometric interpretation. The Doppler frequency is given by the dot product of the pointing or observation unit vector (depending on observation angle) and the spacecraft velocity vector. Therefore, there is a unique correspondence between the observed Doppler frequency f_D and the observation angle θ_i of the scatterer. This is sufficient to locate scattering centres with respect to "zero Doppler" (nominally at nadir) for each processed burst.

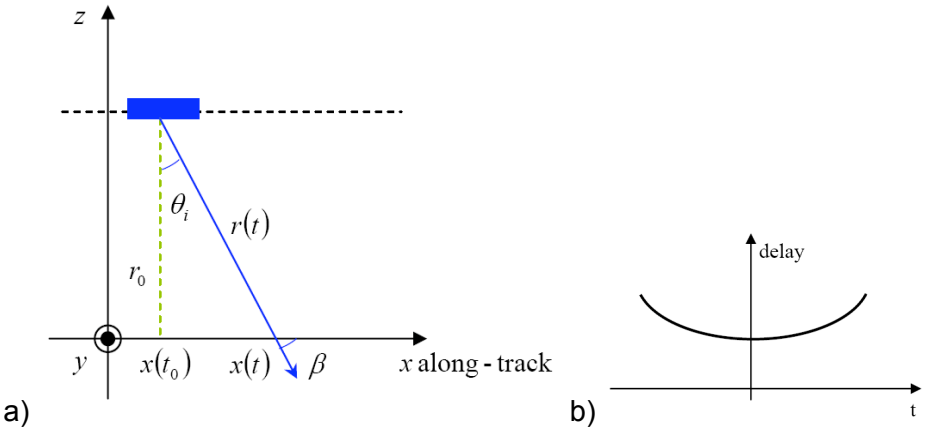

Figure 2-18: a) Along-track scattering point observation; b) Doppler Spectrum geometry

In a simple form, the Doppler frequency can be written as [*Cumming et al.,* 2005]

$$f_D(\theta_i) = \frac{2}{\lambda} \cdot (\vec{p} \bullet \vec{v}_S) = \frac{2 \cdot v_S \cdot \cos(\beta)}{\lambda} = \frac{2 \cdot v_S \cdot \sin(\theta_i)}{\lambda}, \qquad (7)$$

where v_S is the spacecraft velocity. For the range variation ($r(t)$) with respect to the observation angle (again in a simple geometry) applies

$$(x_t - x_0) \approx r(t) \cdot \sin(\theta_i). \qquad (8)$$

Therefore, the Doppler frequency can be approximated as

$$f_D \approx \frac{2 \cdot v_S}{\lambda} \cdot \frac{(x(t) - x(t_0))}{r(t)}. \qquad (9)$$

The position of a scatterer as a function of either time *r(t)* or Doppler frequency *R(f)* follows a hyperbolic law which is known as range cell migration.

$$r(t) = \sqrt{r_0^2 + v_S^2 \cdot (t - t_0)^2}, \qquad (10)$$

where r_0 is the minimum slant range of the satellite to the scatterer, satellite height in this case, and $t_0 \approx x_0 / v_B$ (v_B is the velocity of the altimeter's antenna footprint across the ground) the corresponding over flight time.

Therefore, each Doppler bin represents a unique along-track position of a scatterer.

2.4.3.3 Range Cell Migration Correction

The correction of the range cell migration is necessary in order to place all observations of a scatterer at the same radar range. The relative delay $\delta(t)$ of a given scatterer can be derived form Equation [10] as follows[1]:

$$\delta(t) = r(t) - r_0 = r_0 \cdot \left[\sqrt{1 + \alpha \cdot \frac{(x(t) - x_0)^2}{r_0^2}} - 1 \right], \qquad (11)$$

Where α is the orbital factor ($= V_S / V_B$). After some manipulation and the expansion of the square root in Taylor series, the next simplified expression is obtained,

[1] Note that this is the first time that circular orbital geometry and earth curvature are considered.

$$\delta(t) \approx \frac{\alpha}{2 \cdot r_0^2} \cdot \left(x(t) - x_0\right)^2 . \qquad (12)$$

This factor is applied to each Doppler bin for the range cell migration correction (RCMC). Note that the RCMC shall be applied in the Doppler domain. In this domain, each Doppler bin receives a known RCMC correction that is proportional to the square of the Doppler frequency (relative to zero-Doppler at nadir).

2.4.3.4 Doppler Shift

At this stage, the range migration has been compensated. However, the information from a scatterer still remains at a different Doppler bin for each processed burst. A Doppler shift places the information of a scatterer in the same Doppler bin allowing for unfocussed SAR processing.

2.4.3.5 Inter-burst (incoherent) Accumulation

In conventional altimetry within each burst there will be several looks (one per pulse within the burst). SAR altimetry also maintains the previous looks, and due to its along-track geometry this technique will add additional looks with respect to a conventional altimeter, since the scatterer will be visible in different subsequent bursts.

Using the Doppler shift the along-track looks will be detected, accumulated and averaged to reduce speckle noise effects. The information from a scatterer after averaging will transform into a sharp waveform, Figure 2-19. Note that the along-track accumulation corresponds to an unfocussed SAR compression, i.e. the quadratic Doppler phase modulation due to the movement of the platform does not need to be compensated.

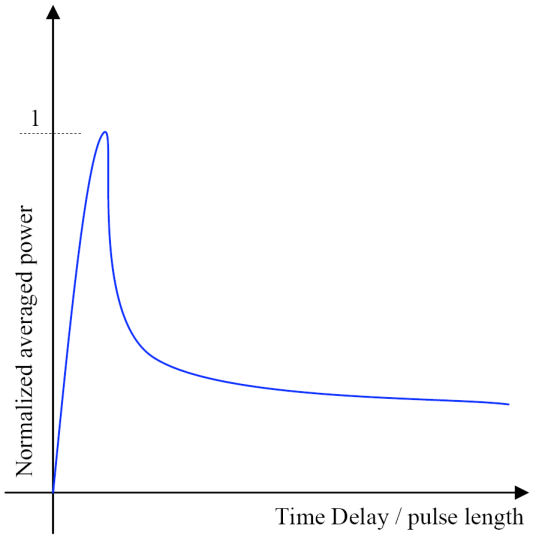

Figure 2-19: Normalized Average power. Image acquired [*Raney,* 1998]

2.4.3.6 SAR Altimeter block diagram

Figure 2-20 reproduces the delay/Doppler altimeter block diagram [Raney, 1998]. The new blocks with respect to Figure 2-12 are highlighted in blue.

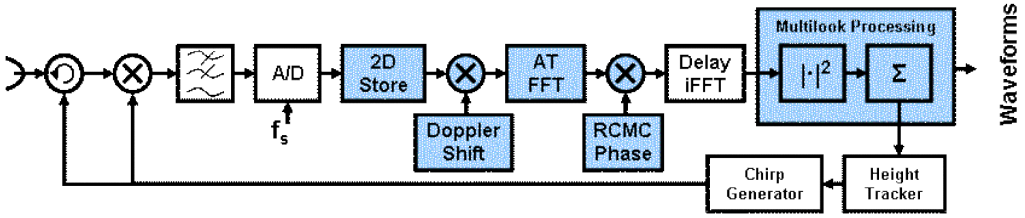

Figure 2-20: Delay/Doppler Altimetry Block diagram.

Note that Doppler shift is performed by multiplication of the along track lines with a constant phase factor in the delay/along-track domain based on Fourier theory. After the along-track FFT, the range cell migration compensation (RCMC) is carried out by multiplication of the range lines with a constant phase factor in the delay-Doppler domain. Finally, after the completion of the range compression, the Doppler bins coming from different burst are detected and averaged for SNR optimization.

2.4.4 SAR Altimetry Performance vs. Conventional Altimetry

SAR altimetry, unlike conventional altimetry, is not pulse limited but Doppler-beam limited. In essence [*Raney,* 1998], SAR altimetry benefits from all the data within the 3dB antenna pattern.

For all Doppler-delimited neighbourhoods near nadir (zero-Doppler), the range data can be converted into ranges relative to that at zero Doppler. Under this condition, the range waveforms at different Doppler delays, once range-compensated, can be combined with the nadir (minimum range) range reference, thus focusing the power in many Doppler bins onto the desired measurement. As long as the radar is constrained to equate zero Doppler with nadir beam-pointing, the height measurements have the same space-craft attitude robustness as conventional pulse-limited altimeters.

2.4.4.1 Signal-to-noise ratio

The SNR of the delay/Doppler altimeter is increased by the contribution of the complete antenna pattern in along-track. In across-track, the pulse length remains as upper threshold of the range integration time.

The SNR of a pulse compressed radar is given by:

$$SNR = \frac{P_T \cdot G^2(\xi) \cdot \lambda^2 \cdot C_R \cdot \sigma^0 \cdot A_\sigma}{(4\pi)^3 \cdot r(t)^4 \cdot N} \qquad (13)$$

where P_T is the transmitted power, G the antenna gain, λ the wavelength, C_R the range compression factor or time bandwidth product, σ^0 the nadir radar backscatter, A_σ area of the resolved footprint, r the slant range distance to the scatter or satellite height h in this case, and N the noise power.

Assuming that both altimeters have identical system parameters, the only difference in SNR of a pulse-limited altimeter and a SAR altimeter is the area of the resolved footprint.

The area of the footprint for the pulse-limited altimeter is given by [*Raney,* 1998]:

$$A_{PL} = \frac{\pi \cdot c \cdot \tau_p \cdot h}{\alpha} \qquad (14)$$

Where τ_p is the transmitted FM pulse length and α the orbital velocity factor. This is basically of the form $A_{PL} = \pi \cdot R^2$, with R the limiting circle for a quasi flat surface response function on a spherical earth

associated to the pulse length. Note that slant range to the scatterer *r* has been substituted by the satellite height *h*.

In addition, the area of the footprint for a delay-Doppler altimeter is given by [*Raney,* 1998]:

$$A_{DD} = 2 \cdot h \cdot \beta \cdot \sqrt{c \cdot \tau_p \cdot h \cdot \alpha} \qquad (15)$$

where β is the along-track antenna beam width. This equation essentially reflects the fact that data and power are collected during the entire time the observation cell is visible by the antenna. This is the crucial difference from conventional altimetry.

Considering the previous equations, the improvement in terms of SNR is directly dependent on the footprint areas for each altimetry concept.

$$\Delta SNR = \frac{A_{DD}}{A_{PL}} = \frac{2\beta}{\pi} \cdot \sqrt{\frac{h \cdot \alpha^3}{c \cdot \tau_p}} . \qquad (16)$$

Note that the relation given in equation 16 is derived from a high-level theoretical approach, and that in practice results are unlikely to provide the level of improvement this suggests. Indeed, one of the purposes of this project is to derive a more rigorous estimate of the expected improvement in SNR using simulated data.

2.4.4.2 Footprint

In contrast to conventional altimeters (see Section 2.3) a SAR altimeter has two independent dimensions: along-track and across-track (range). After SAR processing, these two variables describe an ortho-normal data grid as shown in Figure 2-21.

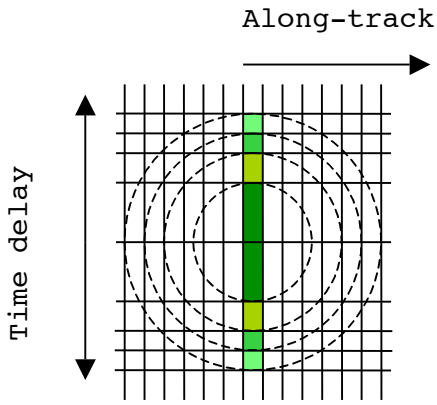

Figure 2-21: delay/Doppler altimeter footprint

The actual nadir point is located in the Doppler bin correspondent to zero Hz and ideally, it is equivalent to along-track position of the satellite. Vertical spacecraft velocity will add Doppler shift to the signals, which should be compensated in order to avoid unwanted along-track shift of the data positions.

The Doppler frequency bin Δf_D is defined from the pulse repetition frequency PRF and the number of pulses per burst N_B

$$\Delta f_D = \frac{PRF}{N_B} . \qquad (17)$$

The along-track altimeter resolution Δx is determined by the scatter illumination time, i.e. the burst length τ_B; and it can be defined as,

$$\Delta x = \frac{v_B}{B_P} \tag{18}$$

with v_B the velocity of the beam or footprint velocity, and B_P the equivalent Doppler bandwidth processed which can be defined under some considerations as:

$$B_P \approx k_R \cdot \tau_B \approx \frac{2 \cdot v_s^{\,2}}{\lambda \cdot h} \cdot \tau_B \tag{19}$$

k_R is the Doppler rate, widely use in SAR processing. Therefore, the along-track resolution can be written as

$$\Delta x \approx \frac{v_B}{2 \cdot v_s^{\,2}} \cdot \frac{\lambda \cdot h}{\tau_B}. \tag{20}$$

Assuming that $V_B = V_S$ and introducing the round-trip delay time T_R, the along-track resolution can be finally written as in [*Raney,* 1998]

$$\Delta x \approx \left(\frac{c \cdot \lambda}{4 \cdot v_s} \right) \cdot \frac{T_R}{\tau_B}. \tag{21}$$

As result the along track footprint is reduced in comparison to conventional altimetry.

2.4.4.3 Timing Constraints

As already mentioned in Section 2.4.2 the delay/Doppler radar altimeter needs pulse-to-pulse coherence within one burst (necessary to support along-track FFT). Thus, it requires a pulse repetition frequency *PRF* higher or equal to the equivalent system Doppler bandwidth B_D driven by the antenna length *L*.

$$PRF \geq B_D = \frac{2 \cdot v_B}{L} = \frac{2 \cdot v_B \cdot \beta}{\lambda}. \tag{22}$$

On the other hand, the transmitted pulse length τ_p constrains the maximum allowed PRF

$$PRF < \frac{1}{\tau_p}. \tag{23}$$

The number of pulses per burst N_B is defined as

$$N_B = \tau_B \cdot PRF\ . \tag{24}$$

with τ_B the burst length, usually equal or lower than the round-trip delay time T_R

$$T_R = \frac{2 \cdot h}{c}. \tag{25}$$

Therefore, assuming that v_B is equivalent to T_R, the number of pulses per burst N_B is constrained by:

$$\frac{4 \cdot h \cdot v_B}{c \cdot L} < N_B < \frac{2 \cdot h}{c \cdot \tau_p}. \tag{26}$$

2.5 Summary

In summary, SAR mode altimetry offers the potential following improvements with respect to conventional altimetry:

- Increment of efficiency of height estimation

- Reduction of footprint dimension in along track
- Smoothed speckle noise with respect to conventional altimeters
- Increment of ca. 10 dB in signal to noise ratio (the delay/Doppler altimeter integrates much more instrument's radiated power).

To smooth the speckle noise pulse to pulse coherence needs to be satisfied, the obverse of that required in conventional altimetry.

SAR mode has been proved to be a realistic and efficient solution for missions like D2P [*Raney & Jensen*, 2001] and in the Cryosat design phase.

The main focus of SAMOSA is to further investigate the application of the DD Algorithm to over-water observations (open ocean, coastal ocean and inland water).

Previous work on SAR altimetry return waveforms modelling is limited. The approach applied in this study will use the work by *Phalippou and Enjolras* [2007] as a starting point. This innovative approach to the SAR altimetry mode waveform model is similar to that of [*Brown*, 1977] and [*Hayne*, 1980]. According to Phalippou and Enjolras the waveform model can be defined as:

$$W(x_i,t) = P_{FS}(x_i,t) * RIR(t) * q_s(t)\,. \qquad (27)$$

Where $P_{FS}(x_i,t)$ is the average flat surface impulse response, RIR(t) the impulse response of the radar or radar system point target response, and $q_s(t)$ the sea wave height probability density function.

Considering, like [*Brown*, 1977] and [*Hayne*, 1980], $q_s(t)$ to be Gaussian for ocean observations; $P_{FS}(x_i,t)$ and $RIR(t)$ can be achieved by analyzing the response of the Delay/Doppler algorithm to an input chirp.

In addition, the use of the delay/Doppler altimeter improves the range accuracy, i.e. the performance of the re-tracking of SAR altimeter waveforms. As shown in [*Peebles*, 1998], a simplified form of the Cramer-Rao bound can be written as

$$\sigma_{CR}{}^2 \geq \frac{1}{N \cdot SNR \cdot W_g^2}\,. \qquad (28)$$

with σ_{CR}^2 being the variance of the re-tracking estimator, *N* the number of samples averaged, SNR the signal-to-noise ratio and W_g^2 the Root Mean Square (RMS) bandwidth of the signal spectral density.

Therefore, due to the improvement in SNR as well as to the new waveform model [*Phalippou and Eljolras*, 2007], the minimum attainable range accuracy is higher. The same authors showed that the range accuracy is improved by a factor 2 upon conventional altimeter for a Poseidon class altimeter.

3 OBSERVING CAPABILITIES OF SAR MODE ALTIMETERS OVER OPEN OCEAN

3.1 Accuracy, precision and resolution

In this section we discuss the improvements in the observations of the open ocean expected from SAR altimetry. Section 4 then deals with the improvements over the coastal ocean. It is appropriate to open these applications sections with a concise discussion of accuracy, precision, and resolution.

We assume that the altimeter's measurements are sample values from probabilistic distributions. Then *accuracy* is the relationship between the mean of measurement distribution and its "true" value, whereas *precision*, also called reproducibility or repeatability, refers to the width of the distribution with respect to the mean. The following figure illustrates these concepts graphically:

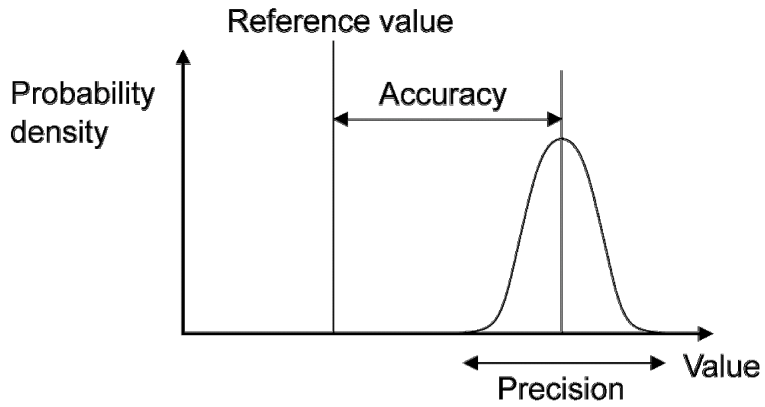

Figure 3-1 Illustration of the concepts of accuracy and precision. The reference value is the 'true' value of the measured quantity. From Wikipedia (http://en.wikipedia.org/wiki/Accuracy)

The dominant context in oceanic altimetry is the measurement of Sea Surface Height (SSH), in which not only the instrument characteristics, but also orbit knowledge, estimation (or measurement) of propagation delays (caused by water vapour or electron density) and their subsequent compensation, and correction for sea surface phenomena (such as EM bias) all play a central role and combine (to variable extent, as explained below) to determine the accuracy and precision of the height measurement. While ideally we would want both accurate and precise measurements, the exact requirements then depend on the application. For instance, the estimation of the rate of global sea level rise from altimetry requires accuracy, but not necessarily precision given the huge numbers of measurements available to compute the mean rate. Instead, studies of El Niño require both accuracy (to discriminate the anomalous raised or lowered SSH value with respect to the mean) and precision, while the detection of fronts or bathymetric features requires only precision.

The above distinction is important also for measurements of SWH and wind speed. Accuracy and precision of these measurements (both desirable, in particular accuracy which is key to assess wind and wave climate trends) do not depend on the accuracy of SSH measurements. Their precision benefits from improved height precision, expressed as smaller standard deviation of the measurement data.

In a satellite altimeter measurement system, range accuracy depends primarily on orbit determination and ancillary measurements (propagation delays, EM bias, etc) and their relevant instrumentation (for instance the microwave radiometer for the determination of the wet tropospheric correction), whereas precision depends primarily on the radar itself. Thus, the measurement benefits of a SAR/DD altimeter are expressed in better precision, but are virtually irrelevant for matters of accuracy. The dominant

factor in a given altimeter's precision is "measurement uncertainty", which is an instrument artefact. This uncertainty is dominated by "speckle", which is reduced by increased averaging of statistically independent samples of the same measurement.

Finally we define resolution as the inverse of the footprint size (in the along-track direction, for example), as opposed to the radar's single-pulse range resolution (for an altimeter the range bin is on the order of 0.5 m width, which in turn is 1/(radar bandwidth)). Note that in non-technical language we often refer to 'resolution' as the width of the spatial cell (footprint or range bin), i.e. we say for instance 'a resolution of 250 m' in space or 'a resolution of 5 cm' in range, but strictly speaking resolution is the inverse of those quantities (so that higher resolution correctly means more samples per unit space, i.e. smaller cells).

3.2 Beneficial aspects of SAR altimetry over open-ocean

A SAR (Delay-Doppler) altimeter retains one of the positive features of conventional pulse-limited altimetry, i.e. the fact that the accuracy in the SSH measurements does not depend (to first order) on pointing accuracy and control/knowledge of the spacecraft attitude. This feature of the Delay-Doppler (DD) technique is redundant for the instrument on CryoSat, which has to meet very strict pointing requirements anyway, due to its interferometric capabilities [*Francis, 2002*], but might prove crucial for the feasibility of low-cost pure-DD instruments to be flown in a constellation.

As described in Section 2, three other features are unique of the DD technique and provide a significant advantage over conventional instruments [*Raney,* 1998]:

a) the along-track length of the instantaneous pulse-limited footprint is constant (does not depend on SWH);

b) a greater number of looks than in a conventional altimeter are accumulated over each along-track location, resulting in better signal-to-speckle ratio, SSR[2], (smaller measurement standard deviation) at the same posting rate of a conventional altimeter;

c) the SSR improvement allows an increase of the sample posting rate which results in a shorter (and not dependent on SWH) footprint along-track length (the lower limit for this is the length of the instantaneous pulse-limited footprint,~285 m for CryoSat). But note that shorter posting rates imply proportionately fewer independent samples, and hence larger SSR, so that a trade-off must be chosen depending on the particular application.

The performance of the instrument in terms of height measurement precision has been first analyzed by *Jensen and Raney* [1998]. At 1Hz posting rate the precision of the range measurement is improved by a factor 2 with respect to a conventional altimeter. This improvement has been confirmed by *Phalippou and Enjolras* [2007]. *Francis* [2007] analyzes in some detail the error budget of Sentinel-3 SRAL and quotes a 0.8 cm height noise for the Ku-band SAR altimeter for a SWH of 2m. The potential improvement in range accuracy then depends critically on the quality of the corrections, in particular the ionospheric correction (CryoSat is single-frequency instrument) and the wet tropospheric correction (CryoSat lacks a microwave radiometer on board), as discussed in more details below.

The improved SSR has beneficial effects also on SWH, for which *Jensen and Raney* [1998] found a precision (precision meaning here the standard deviation solely from an instrument processing perspective) of ~1cm at 1Hz almost independent on the SWH value, which represents a significant improvement over conventional altimetry for sea conditions moderate or stronger. Wind speed estimation is also more precise by about 20%, and also shows a greater improvement for larger SWH.

The same simulations by J.R. Jensen [*ibid*] show that the performance of the SAR altimeter in estimating the three basic parameters is almost unaffected by the presence of receiver noise at the 10dB SNR level.

---

[2] The Signal to Speckle ratio (SSR) is relevant here rather than the Signal to Noise Ratio (SNR). For almost all oceanographic radar altimeters, SNR proper is only of secondary concern, if at all. Precision is driven by the self-noise known as speckle, which in fact is not additive, but rather is multiplicative, thus proportional to signal strength.

All these features can be usefully exploited over the open ocean to push forward the boundaries of what altimetry can do. New and improved applications can take advantage either of the enhanced along-track resolution, or of the enhanced precision, as well as of any desired trade-off amongst those two characteristics. In the following we list the phenomena that can be observed, from the largest scale (spatial scales > 500 km to the mesoscale (scales of 10-500 km) to the small scale (scales < 10 km) with a description of the relevant capabilities that should be exploited.

3.3 Observable phenomena in the open ocean

A very useful overview of oceanic phenomena based on their temporal and spatial scales is in *Chelton* [2001] and is summarized in figure 3.2 redrawn from that report, where we have superimposed a box spanning the range of scales that are in principle observable with the CryoSat SAR altimeter.

3.3.1 Large- (≥ 500 km) to meso-scale (10-500 km)

Conventional altimetry has been extremely valuable in the observation of the dynamics of the open ocean at wide range of spatial and temporal scales [*Fu and Cazenave*, 2001]. In particular, it has been successful in monitoring both planetary waves [*Chelton and Schlax*, 1996] [*Cipollini et al*, 2006] and the meso- to large- scale eddy field [*Chelton et al*, 2007]. Any DD altimeter can contribute to extending the measurements of those features provided that the geoid signal can be removed, which can be attempted by analysis of crossovers with respect to instrument in short-repeat orbit such as Jason-1 and EnviSat.

Of perhaps greater importance is the estimation of the open ocean wave and wind field from CryoSat, which should result in a dramatic improvement of the existing climatologies. In some cases (notably wind speed) present-day sampling is inadequate for a complete monthly climatology at a scale appropriate to the auto-correlation length scale [*Cotton et al.,* 2004]. Any satellite that adds to this sampling would be welcome, and the resulting improved near-real time capability is paramount for shipping and offshore operations.

However, this project is targeted at investigating the opportunities at improved measurements offered specifically through the SAR altimeter mode technique. Therefore we shall focus subsequent discussions on this aspect.

With respect to larger scale oceanic phenomena, the expected higher precision of DD-derived wind speeds and wave heights [*Jensen and Raney,* 1998] would allow better estimates of air-sea fluxes (in particular the estimation of global mean air-sea gas transfer velocities) whose climatologies are centrally important in climate studies [*Cotton et al.,* 2004]

3.3.2 Smaller scale (< 10 km)

A number of phenomena in the open ocean are yet unresolved by conventional 1 Hz altimetry, and can potentially be observed in virtue of the higher along-track resolution of SAR altimetry. In principle, many of the features with scales greater than a few hundred meters that are visible in SAR imagery (see for instance ch. 10 of *Robinson* [2005]) should appear in the high-resolution along-track backscatter (σ^0) measurement taken by a DD altimeter. Amongst these are internal waves and internal tides (see figure 3-3), important for ocean mixing, as well as natural or man-made slicks. As all those phenomena provoke rapid variations of σ^0, so there is clear scope for studying the response of the instrument to such rapid variations. Also the effects of rain cells (see below) and other atmospheric phenomena such as small-scale wind bursts and convective cells in an unstable atmospheric boundary layer may result into abrupt variations of σ^0 [see several examples of this in *Alpers et al*. 1999, from which Figure 3-3 is taken]. These considerations have instructed some of the simulation scenarios detailed in section 3.4.

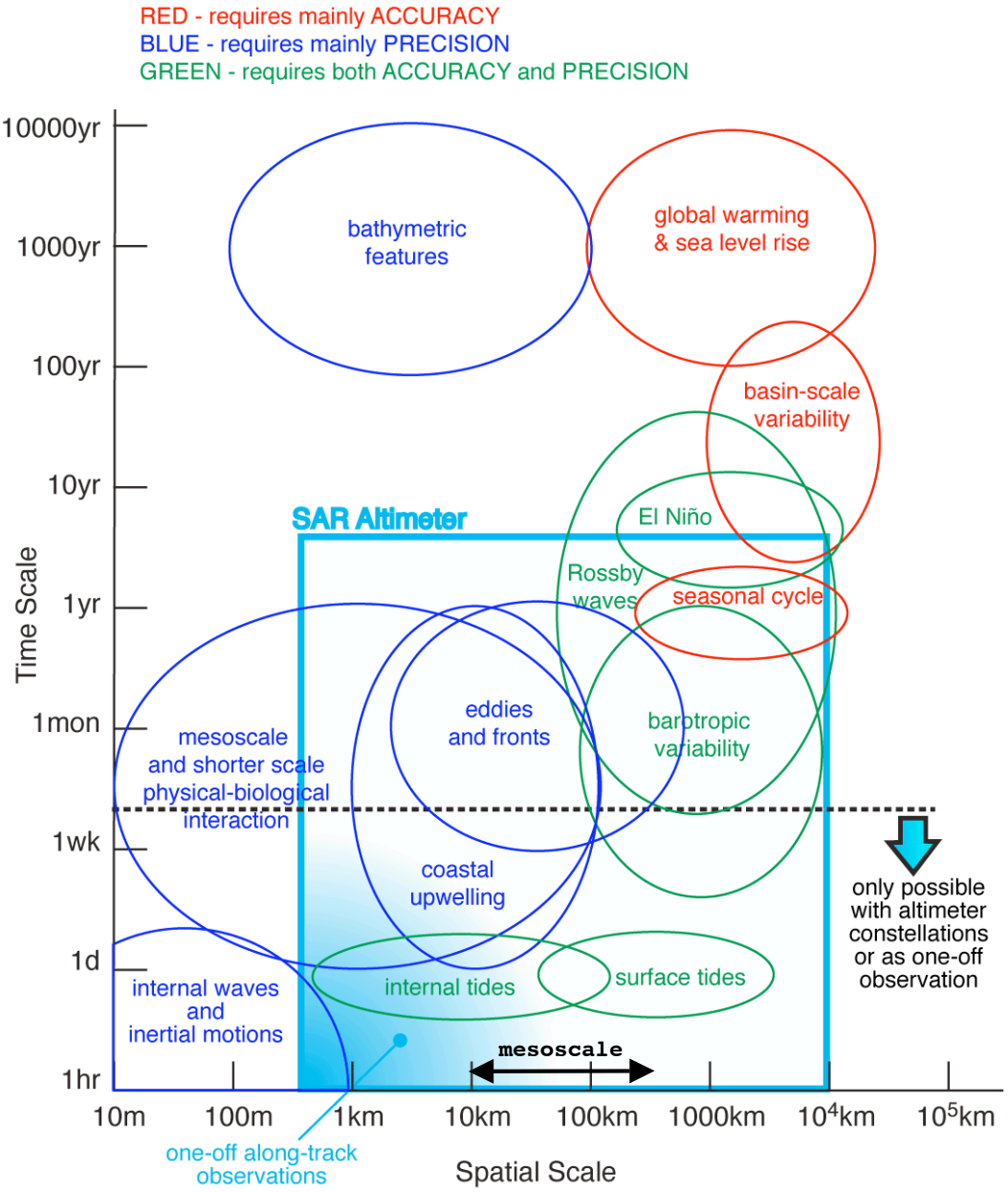

Figure 3-2 From [*Chelton,* 2001] re-drawn and extended. Space and time scales of phenomena of interest that could be investigated from altimetric measurements of ocean topography with adequate spatial and temporal resolution, The dashed line indicates the approximate lower bound of the time scale resolved (with repeated observations) by a single nadir-viewing altimeter mission. The cyan square encompasses the overall range of scales that can be resolved by a single non-repeat SAR altimeter (in this case for the lower bound of the spatial scale we have used the along-track resolution). The cyan shaded area indicates ranges that can be resolved by one-off along-track observations. Phenomena are color-coded according on whether their observation mainly requires accuracy (red), precision (blue) or both (green). This colour classification is an original contribution of this study.

Figure 3-3. ERS-1 SAR image of the South Tyrrhenian Sea and Messina Strait taken on 8 September 1992, when the sea temperature was ~25°C and air temperature ~16C. This image shows the σ^0 signature of several phenomena that can in principle be observed by DD altimetry. Note in particular the bright signature of katabatic winds from the north coast of Sicily and Calabria, the small-scale eddy made visible by spiral patterns of surface slicks, the large area interested by small convective cells between Sicily and the island of Stromboli in the north, and the train of internal waves south of the Messina Strait. From [*Alpers et al., 1999*]

3.3.3 New Observables and relevant requirements

Rain Cell size distribution

Rain cells cause sharp decreases in the observed σ^0 in Ku-band [*Guymer et al.,* 1995], [*Quartly,* 1998]. The size of the rain cells obtained from measurements over land is well described by an exponential distribution [*Sauvageot et al.*,1999] with slopes around 0.2-0.4 km^{-1}, which makes km-scale cells highly likely. The DD altimeter can therefore be employed to investigate the size distribution of rain cells over the open ocean.

Sea surface skewness

We refer here to wave skewness and short-scale skewness of the sea surface (meso-and large-scale skewness, i.e. skewness at scales of tens and hundreds of km, can be readily estimated from gridded data – see *Thompson and Demirov* [2006]). Wave skewness can be estimated from re-tracking assuming a nonlinear statistic for the ocean waves [*Gomez-Enri et al,* 2007]. Sea Surface Skewness retrievability in SAR altimeter echoes can only be tested with CRYMPS by providing as input a sea surface that accounts for non-zero skewness. This opportunity will be discussed in Phase 2 of the SAMOSA project.

Long swell waves

For extremely long wavelength swell, exceeding the 570-m Nyquist wavelength, in principle some signal could become observable. There is also scope for investigating how detectability depends on the relative orientation of the wave fronts with respect to the satellite track. We need to test this scenario with a dedicated CRYMPS simulation, which will be designed in Phase 2 of the Project.

3.3.4 Summary of SAR mode Altimetry measurements over the open ocean

Measurements that benefit from increased precision:

- SWH
- Wind field
- meso- to large- scale eddy field (only in combination with short-repeat instruments).

Measurements that benefit from increased resolution:

- fronts
- small-scale eddies
- slicks
- gradients in wave height close to the shore.

New observables

- Rain cell size distribution
- wave skewness
- long swell (to be tested)

3.4 CRYMPS simulation scenarios for the open ocean

3.4.1 CRYMPS overview

The CryoSat mission performance simulator (CRYMPS) simulates the CryoSat platform orbit, characterises a surface in order to generate field echoes, simulates the instrument operation and generated products (only the binary part without headers) for all 3 modes (SAR/SARin/LRM).

CRYMPS has been conceived to simulate the response of the instrument over ice; an important implication of this is that the simulated surface does not move during the satellite overpass, i.e. it is 'frozen'.

Before launching CRYMPS, a Digital Elevation Model (DEM) has to be selected. CRYMPS DEMs are regular grids in lat/long containing either a) geodetic heights (specified with respect to a reference ellipsoid) or b) geodetic heights, backscatter σ^0 and polar angle (variation of the backscatter with the angle from the normal – for ocean runs this can be taken as constant and equal to 0°).

In terms of representation of surface waves, CRYMPS only allows the direct prescription of the amplitude and wavelength of a **single 'swell' spectral component** (originally introduced to reproduce the undulating topography of some ice sheets). This problem can be circumvented by generating an appropriate DEM either with prescribed multiple wave components, or from the inversion of a realistic wave spectrum (as in scenarios C1-C3 see below). However it must be remembered that the limitation of a 'frozen' surface holds.

Another input parameter is the standard deviation of the Gaussian white noise that CRYMPS add to the DEM. This has the same distribution over the entire domain on which the simulation is run; changing (and/or non-Gaussian) noise patterns can however be accounted for by incorporating them in the DEM in the first place.

3.4.2 Strategy from commissioning CRYMPS simulations

The strategy for the commissioning of the all CRYMPS simulation, over open ocean, coastal ocean and land, is the following:

1) run a first batch of simulations over a small number of simple, idealized scenarios to be run as soon as possible, so that the project partners can have a quick look at the CRYMPS data and gauge the performance of the CRYMPS simulator and its suitability for this task. The scenarios for the first batch are denoted with F and a number (for the open ocean, see §3.4.3) and with SFT and a number (for gravity mapping purposes, see §3.5.4). To these are also added three scenarios deriving from the inversion of a realistic wave spectrum, which we denote with letter C and a number.

2) subsequently, run a second batch of simulations with more realistic parameters (for instance, taking the configuration of the different kind of surfaces from real cases, or simulating islands, fronts, etc). These scenarios are detailed in §3.4.4 and §4.3 and some of their parameters are subject to fine tuning once the results of the first batch are analyzed.

3.4.3 First batch scenarios

The CRYMPS simulation scenarios for the open ocean described in this sub-section have been designed based on the following assumptions:

- 8-second scenarios (so that each one covers ~54 km along-track);

- each scenario has constant swell amplitude and wavelength;

- scenarios F1 to F4, and F6 have constant σ^0, while scenario F5 has changing parameters with respect to the scattering surface to investigate the impulse response and step response of the instrument.

- scenarios C1 to C3 derive from the inversion of a realistic wave spectrum.

L1 SAR mode output will be required for all these scenarios, in addition to L1B and L2 SAR mode and LRM mode.

Scenario F1

- swell amplitude = 1m, wavelength = 100m and PDF s.d. = 4cm;

a swell amplitude of 1m broadly corresponds to a SWH of 1.41 m. These conditions (shown as F1 in figure 3.5) approximately correspond to those encountered by the airborne SAR altimeter ASIRAS during the CRYOVEX 2006 experiment on 2 May 2006 (SWH = 1 to 1.7m, Tz ~ 5 to 6.5 s). This scenario has been then merged with scenario F3 (see below).

Scenario F2

- swell amplitude = 3m, wavelength = 150m and PDF s.d. = 10cm;

a swell amplitude of 3 m approximately corresponds to a SWH of 4.23 m. This scenario has been then merged with scenario F4 (see below).

Scenario F3

- swell amplitude = 0.5m, wavelength = 50m and PDF s.d. = 4 cm;

a swell amplitude of 0.5m approximately corresponds to a SWH of 0.71 m. These conditions (shown as F3 in figure 3-5) broadly correspond to those encountered by ASIRAS during the CRYOVEX 2006 experiment on 30 April 2006 (SWH=0.5 to 1.5 m; Tz approximately 5.5 s). This scenario has been then merged with scenario F1 (see below).

Scenario F4

- swell amplitude = 10m, wavelength = 200m and PDF s.d. = 20cm;

a swell amplitude of 10 m approximately corresponds to a SWH of 14.1 m

this simulates extreme sea state conditions, as a swell amplitude of 10 m approximately corresponds to a SWH of 14.1 m. This scenario has been then merged with scenario F2 (see below).

Merged F1/F3 and F2/F4 scenarios

In consideration of the fact that scenarios F1 to F4 are distinctly uniform along-track, and in order to keep the number of CRYMPS simulation to a minimum, it has been decided by the SAMOSA partners to merge scenarios F1 and F3, and scenarios F2 and F4, as follows:

MERGED F1/F3: 2.5 s of F1, then 3 s of F3, then 2.5 s of F1

MERGED F2/F4: 2.5 s of F2, then 3 s of F4, then 2.5 s of F2

these are designed so that they present transitions both ways (i.e. from calmer to rougher and vice - versa), and still sufficient length of time to assess the response to each separate conditions. The merging is done with no discontinuities in the transitions, so for instance when conditions change from F1 (wavelength=100m) to F3 (wavelength=50m) this happens at a zero-crossing level so that there is no 'step'.

Scenario F5

This scenario, sketched in figure 3-4 below, is designed to study the impulse (150m width) response and the step (10km width) response of the instrument to a change of σ^0, with two different values of $\Delta\sigma^0$: 5dB and 10dB. The swell and noise parameters are as for F1, i.e.:

- swell amplitude = 1 m, wavelength = 100 m and PDF s.d. = 4 cm ;

Scenario F6

This scenario, also sketched in figure 3-4 below, is designed to study the impulse (150m width) response and the step (5km width) response of the instrument to a change of sea surface height, with impulses and steps of ±5 cm and ±10 cm [these are obviously an idealized situation]. The swell and noise parameters are as for F1, i.e.:

- swell amplitude = 1 m, wavelength = 100 m and PDF sd = 4 cm ;

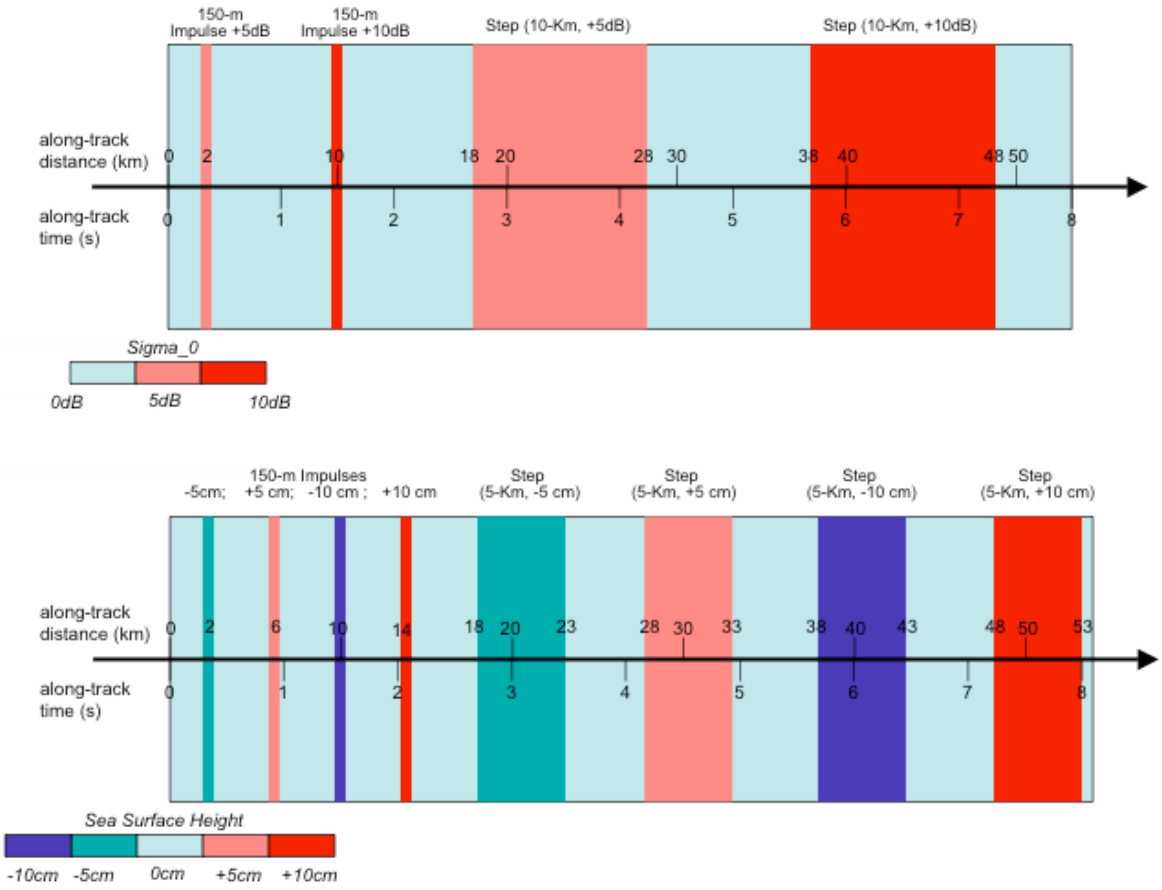

Figure 3-4. Schematic of the CRYMPS scenarios to investigate the instrumental impulse response and step response to variations in σ^0 (scenario F5, upper panel) and in surface elevation (scenario F6, lower panel)

Scenario C1

This scenario is derived from the inversion of an Elfouhaily **omni-directional** wave spectrum [*Elfouhaily et al.*, 1997], with varying peak SWH along track, as follows: 2 s with SWH = 0.1 m, then 1 s of linear transition, 2 s with SWH = 1 m, then 1 s of linear transition, and finally 2 s with SWH = 2 m.

Scenario C2

This scenario is derived from the inversion of an Elfouhaily **omni-directional** wave spectrum [*Elfouhaily et al.*, 1997], with varying peak SWH along track, as follows: 2 s with SWH = 2 m, then 1 s of linear transition, 2 s with SWH = 3 m, then 1 s of linear transition, and finally 2 s with SWH = 4 m.

Scenario C3

This scenario is derived from the inversion of an Elfouhaily **mono-directional** wave spectrum [*Elfouhaily et al.,* 1997], with varying peak SWH along track, as follows: 2 s with SWH = 1 m, then 1 s of linear transition, 2 s with SWH = 2 m, then 1 s of linear transition, and finally 2 s with SWH = 3 m. The direction of the waves is along-track.

N.B. A subsequent decision was taken to run this scenario before C1 and C2

3.4.4 Follow-on scenarios for the open ocean

The CRYMPS simulation scenarios for the open ocean described in this sub-section, are designed to investigate the detectability of the various phenomena described in §3.3 and are based on the assumptions listed below. **These 'follow-on" scenarios are expected to be fine-tuned and consolidated once the data from the first batch of runs have been made available**; in particular, not all of the scenarios detailed below will be run, and some may be merged (in a similar fashion to F1/F3 and F2/F4 in the previous section) to keep the number of CRYMPS run to a minimum. The following assumptions are made:

- 8-second scenarios (so that each one covers ~54 km along-track);

- each scenario has constant swell amplitude and wavelength;

- each scenario can have changing parameters with respect to the scattering surface, at scales of 4-5 km)

The rationale for the design is as follows:

a) with respect to the shape and layout of the features encountered along the 54km track, we adopt a track representative of "fronts" (frontal regions, filaments, elongated wind bursts) and one representative of "cells" (circular-shaped structures as rain cells and convective cells). The two tracks are illustrated in figure 3-5.

b) both the fronts track (code OF) and the cells (code OC) track are simulated for each of the following conditions:

OF1/OC1 SWH = 1m ⇒ swell amplitude = 0.71 m, wavelength = 25m and PDF s.d. = 4cm;

OF2/OC2 SWH = 1m ⇒ swell amplitude = 0.71 m, wavelength = 66m and PDF s.d. = 4cm;

OF3/OC3 SWH = 3m ⇒ swell amplitude = 2.12 m, wavelength = 66m and PDF s.d. = 10cm;

OF4/OC4 SWH = 3m ⇒ swell amplitude = 2.12 m, wavelength = 127m and PDF s.d. = 10cm;

OF5/OC5 SWH = 3m ⇒ swell amplitude = 2.12 m, wavelength = 207m and PDF s.d. = 10cm;

OF6/OC6 SWH = 10m ⇒ swell amplitude = 7.07 m, wavelength = 207m and PDF s.d. = 20cm;

which makes **6 x 2 = 12 simulations in total, denoted OF1 to OF6 and OC1 to OC6**

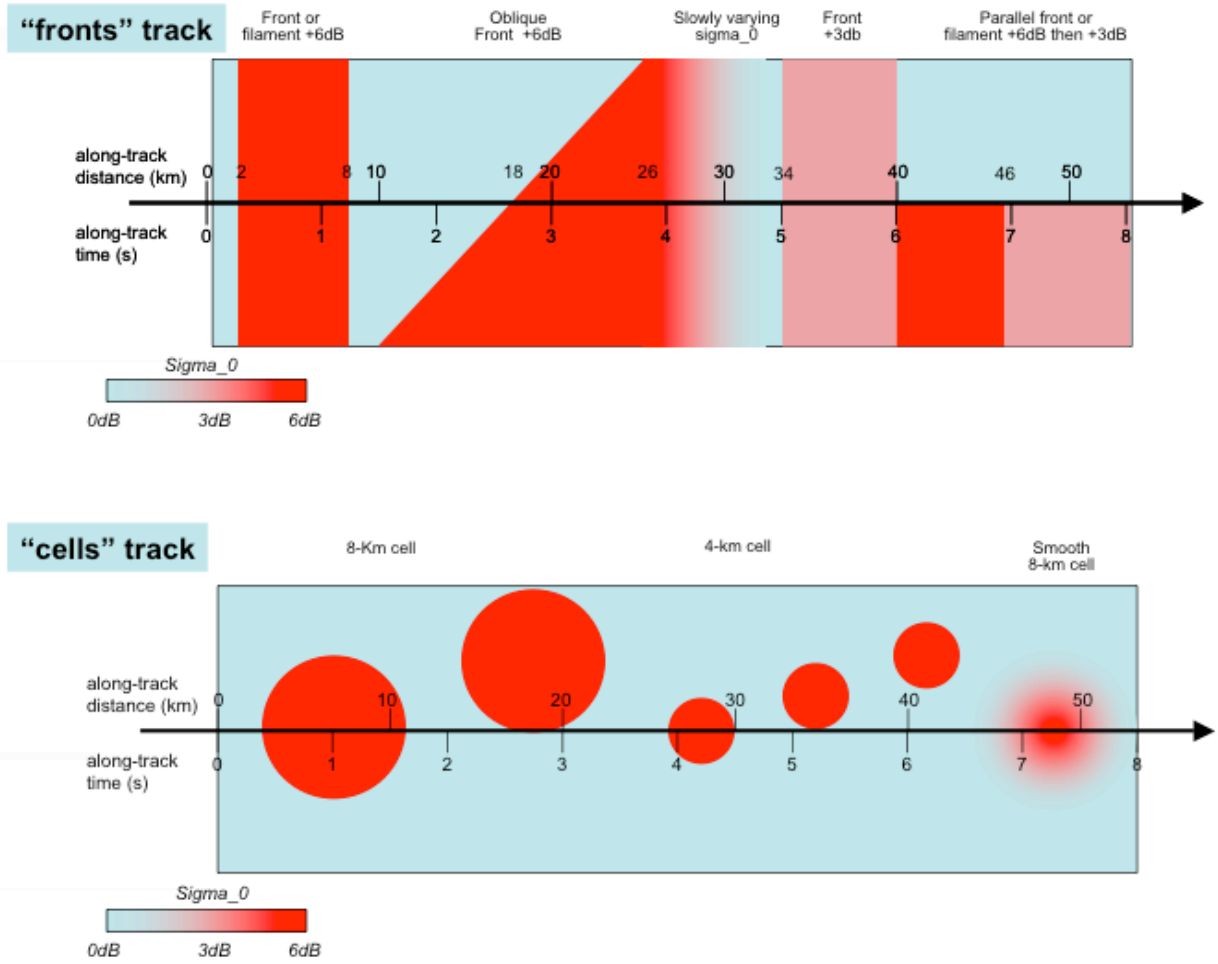

Figure 3-5. Schematic of the fronts and "cells" scenario for CRYMPS simulations over the open ocean.

In the above scenarios the values for the pairs [SWH, wavelength] have been chosen in agreement with the measurements from a collocated altimeter/buoy dataset gathered over more than 15 years [*Mackay et al*., 2008] presented in figure 3-6. The zero-upcrossing wave period T_z in the figure is related to wavelength λ by:

$$\lambda = \frac{gT_z^2}{2\pi}$$

For SWH = 1 m we have taken as typical values of T_z 4.0 s and 6.5 s, resulting in wavelengths of 25 and 66 m, respectively. For SWH = 3m we have adopted T_z = 6.5 s, T_z = 9.0 s and T_z = 11.5 s, resulting in wavelengths of 66, 127 and 207 m, respectively. For SWH = 10 m we have adopted T_z = 11.5 s, resulting in a wavelength of 207 m. The regions of the plot in figure 3-6 representative of these example conditions are marked with a grey star on the plot.

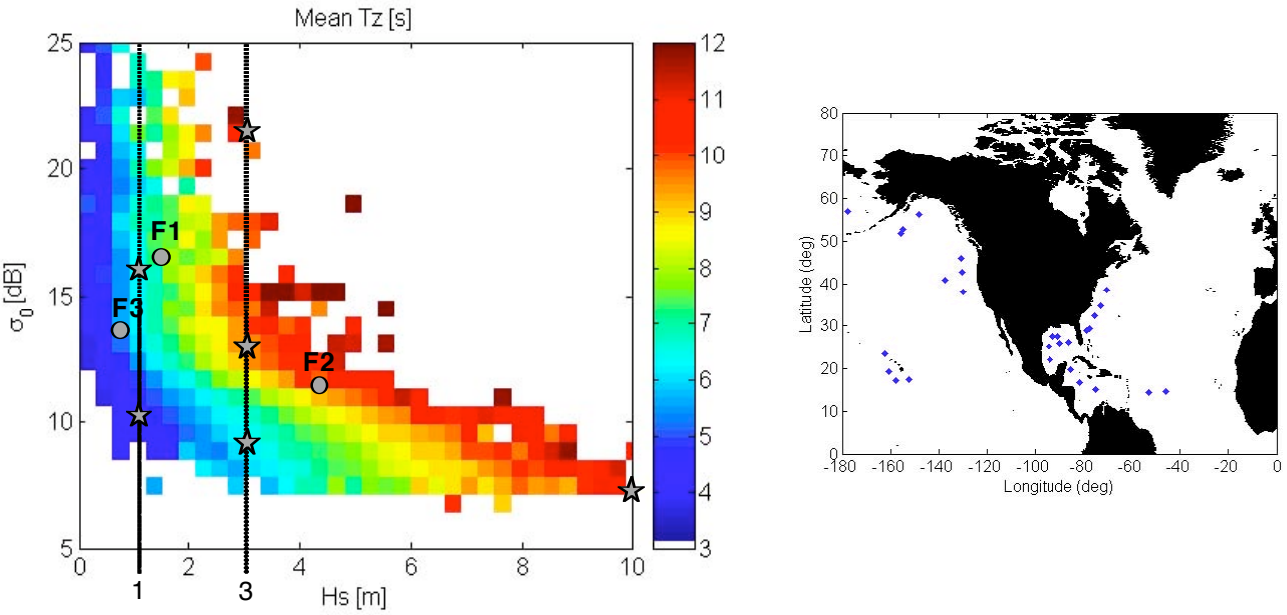

Figure 3-6. (left panel) distribution of σ^0, SWH (in m) and zero-upcrossing wave period (in seconds) from a collocated altimeter/buoy dataset gathered over more than 15 years. (right panel) the location of the buoys used for collocation. The grey circles correspond to conditions for the CRYMPS F1, F2 and F3 scenarios in §3.4.3, and the grey stars mark typical conditions taken as reference for the CRYMPS open ocean scenarios in §3.4,4. From [*Mackay et al*, 2008].

3.5 Measurement of sea floor topography, and gravity field mapping with SAR Mode altimeters

3.5.1 Satellite altimetry for gravity and sea floor topography

The important capability offered by the satellite altimeter to support new mapping of oceanic gravity fields has been recognised and exploited for many years. When using satellite altimetry in this way to calculate gravity anomalies, two approaches have been applied. The “DNSC” technique [e.g. *Andersen et al.,* 2005] uses the along-track heights directly, whereas in the “SS “ technique [*Sandwell and Smith,* 1997] the along track sea-surface height measurements are differentiated to calculate the induced surface slope. Both approaches provide a direct measurement of the geoid changes at the location and consequently also of the local gravity field change. Using gravity inversion techniques the associated sea floor topography can then be deduced. The schematic of how sea floor topography is derived from the height of the sea surface measured by satellite altimetry is shown in Figure 3.7.

Both the SS and DNSC methods require high precision in the individual sea surface height observations because the signal induced at the sea-surface is a filtered and diluted signal of a sea-floor effect, the deeper the ocean, the smaller the signal induced at the surface. However absolute accuracy in height measurements is not so important, due to the along-track differentiation applied in the SS technique, and the fact that the DNSC07 method removes all features longer than 200 km wavelength (or less, if a high resolution geoid is used).

Both approaches will provide higher resolution fields in the along-track direction than in the cross track direction, due to the higher sampling frequency along-track. Thus, to achieve a more complete mapping of gravity fields in all directions, a moderate inclination orbit is to be preferred (see section 3.5.5 for a more detailed discussion).

The SS approach has severe limitations however when applied to data from satellite altimeters on high inclination orbits(e.g. 108° and 98° for GEOSAT and ERS, respectively). At low latitudes, when the satellite ground track runs almost north-south, the geoid slope in the north-south direction is derived much more accurately than the east-west slope. Similarly the north-south slope is less accurate then

the east-west slopes when derived at the turning latitudes of the satellites (see *Sandwell and Smith*, [1997] for details). Consequently the SS method is best applied to altimeter data from satellites on moderate inclination orbits. The DNSC approach is not so sensitive to the orbit configuration, and hence can also use data from an orbit with very high inclination like CRYOSAT.

Satellite altimetry does not provide a direct measure of sea floor topography and satellite observations must be combined with direct observations from ship (e.g. echo soundings) in order to derive accurate sea floor topography maps of the world's ocean. Even though satellite altimetry is combined with marine observations of much lower spatial density the high frequency features can be obtained from the high spatial sampling of satellite altimetry.

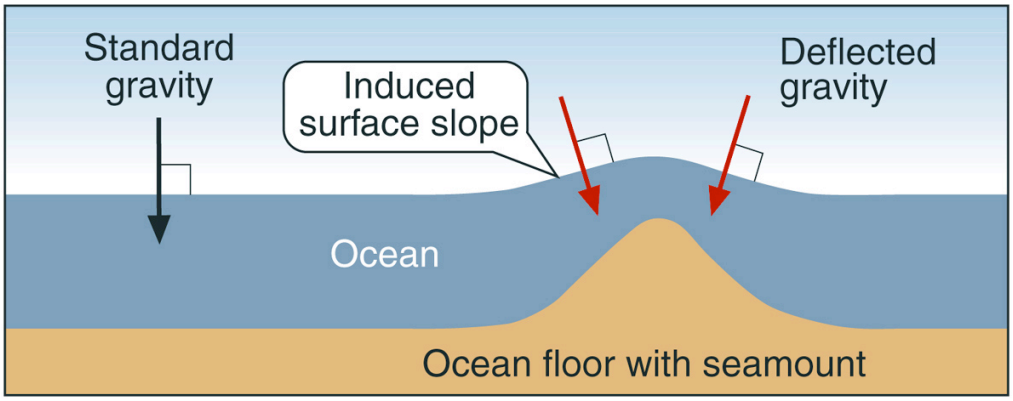

Figure 3-7 The connection between observed sea surface slope and height changes of the ocean from satellite altimetry, gravity anomalies and sea floor topography (from [*Smith*, 2005])

Gravity anomalies are to a large extent associated with sea floor topography and the spatial correlation over the open oceans is larger than 80% in many regions. Consequently gravity field mapping and the charting of sea floor topography is highly connected, and in many regions of the world gravity anomalies are the only practical way of obtaining sea floor topography information.

In order to map the marine gravity field and the sea floor topography one of the key requirements is to obtain the highest possible spatial density and accuracy in the sea surface height observations.

3.5.2 Limitations of current altimetric methods

Gravity field observation and sea-floor mapping from e.g. echo sounding are generally obtained from marine surveys. However two decades ago satellite altimetry revolutionised the mapping of the global gravity field and sea floor topography of the world's ocean, and in most regions of the world the resolution of the available sea floor topography mapping is directly dependent on the resolution and accuracy of available satellite altimetric observations, as shown in Figure 3.8.

Global marine gravity field maps and associated sea floor topography have been mapped using the ERS-1 Geodetic Mission (GM) of the ERS-1 satellite (1994-1995) and the GEOSAT GM (1985-1986). During these GM phases, the altimeter's orbits were non-repeating (Geosat), or constrained to a long repeat period (ERS-1) These observations were fundamentally different to all other current satellite mission like JASON-1, ENVISAT and GFO where the satellites repeat a number of pre-selected ground tracks with a spatial separation between 70 and 350 km.

During the GM the spatial separation of the ground tracks is similar to the along track separation of the 1 Hz observations namely 8 km. Consequently spatial features can be mapped with a spatial resolution down to 16 km. This number will vary spatially in a complex fashion with both latitude and longitude as the sampling was not fully uniform during the GM.

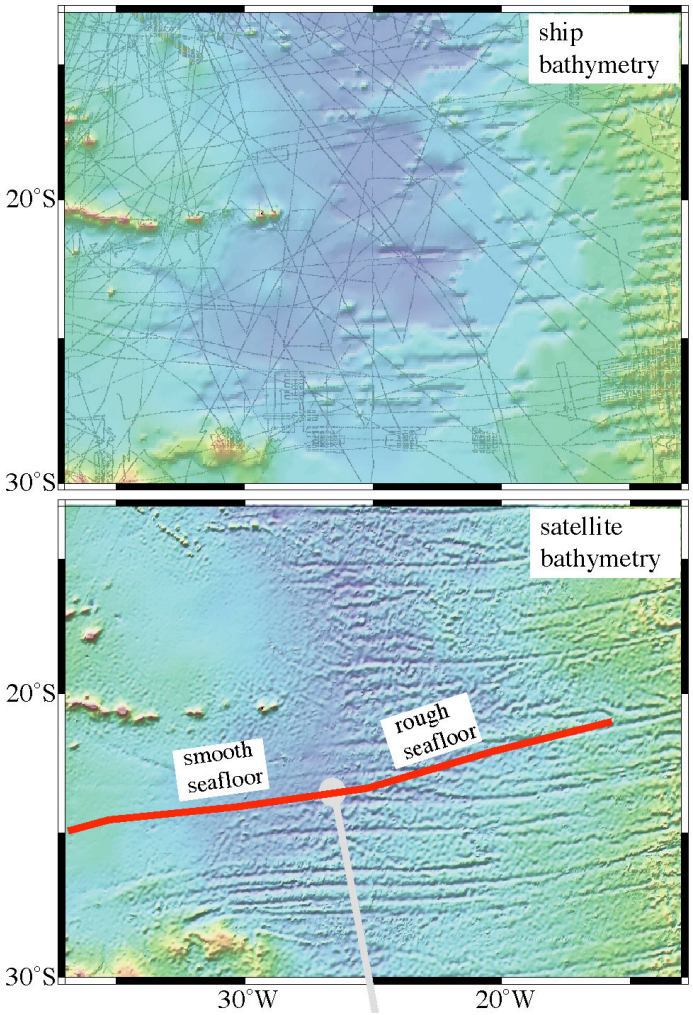

Figure 3-8 Bathymetry charted from existing marine surveys (upper picture) and Bathymetry charted from a combination of marine surveys and satellite altimetry, modified from [*Sandwell et al.,* 2004]

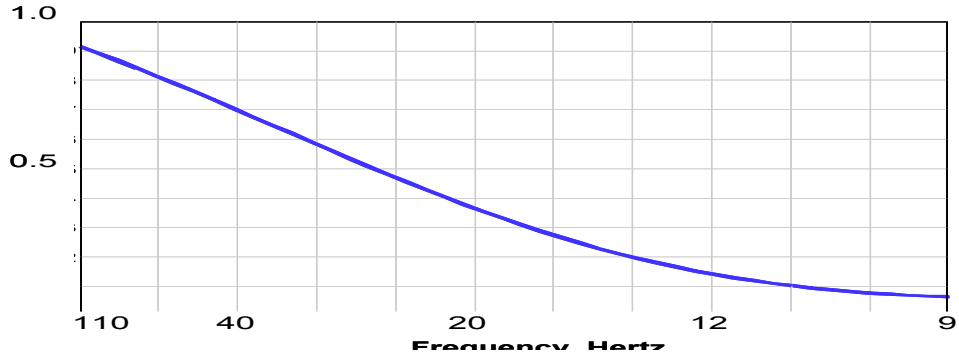

Figure 3-9 Normalised power spectral density from the global marine gravity field KMS02 [*Andersen et al.,* 2005] and [*Andersen and Knudsen,* 1998] for a 400 km NS profile in the central Atlantic Ocean. On the x-axis the wavelength is shown and on the y-axis the PSD is shown normalized to the max power.

A more detailed investigation of the spatial resolution of global marine gravity field and bathymetry derived from satellite altimetry can be found by performing a power spectral density (PSD) analysis of one of the currently most accurate global gravity field maps, the KMS02 global gravity field. This is shown in Figure 3-9.

The KMS02 global marine gravity field derived from satellite altimetry has a spatial resolution of 20-25 km as seen from Figure 3.9 and the 1-hz height observations on which these are based, are given with a standard deviation of 6-7 cm (can be improved through re-tracking). More recent global gravity fields do have a somewhat better resolution (DNSC07 – to be released shortly) due to the use of re-tracking. The DNSC07 has a spatial resolution of around 18 km. This number is currently the limit that can be achieved from conventional satellite altimetry.

Close to the coast the accuracy of the satellite derived gravity fields and sea floor topographies degrades due to several causes [*Andersen et al.,* 2005]. This is clearly shown in Figure 3-10 which presents a comparison between two global marine gravity fields and a global sea floor topography with marine observations for increasing proximity to the coast.

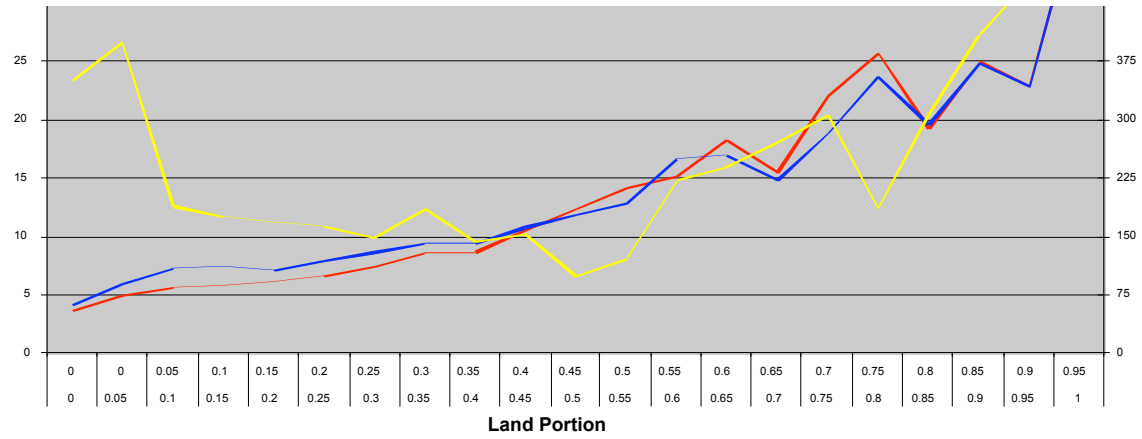

Figure 3-10. Comparison between two global marine gravity fields (blue Sandwell and Smith v 8.2; red KMS02) and a global sea floor topography (SS-Topo 7.2) with marine observations for increasing proximity to the coast. The left scale is discrepancy in mGal for the gravity fields and the right scale is the depth discrepancy in metres. Land portion correspond to the amount of land within a spherical cap with radius of 15 km centred on the location of observation.

In terms of spatial resolution, current altimeter data delineate the large offshore basins and major structures (like plate tectonics), they do not resolve some of the smaller geomorphic features and they cannot be used to detect some of the smaller basins. Wavelengths shorter than 30-40 km in the presently available data cannot be interpreted with confidence close to shore, as the raw altimeter data are often missing or unreliable near the coast. The off-shore exploration industry would like to have altimeter data with as much resolution as possible and extending as near-shore as possible since most sedimentary basins lie close to the shore. The 2-D seismic survey standard in the industry uses a track line spacing of 5 km, yielding structure maps with a 10 km Nyquist wavelength.

3.5.3 Advantages of the Delay-Doppler altimeter

The preceding section has outlined the major limitations of conventional satellite altimetry in deriving accurate marine gravity fields and sea floor bathymetry. The three main issues are: resolution, precision and shoreline proximity.

The Delay-Doppler (DD) in SAR mode provides key improvements to all these issues. More specifically, the DD has three significant advantages over conventional satellite altimetry.

These are

The along track length of footprint is constant and does not increase with significant wave height

The along track resolution is around 300 meter versus 6 km for 1-Hz conventional satellite altimetry.

The precision is improved by a factor of two compared with current-day altimeters.

Furthermore it is important to be aware that existing maps have been derived from geodetic mission altimetry onboard the GEOSAT satellite in 1985-1986 and onboard the ERS-1 satellite in 1994. Current day altimeters are more accurate and the improvement in the DD data compared with these "old" instruments is most likely higher than a factor of two.

The requirements for geodesists/geophysicists for gravity and bathymetric mapping are fundamentally different from the requirements for oceanographic studies. Oceanographers generally want repeated observations along predefined ground tracks for the study of dynamic phenomena. Geodesists/geophysicists want non-repeating observations with the highest spatial density and precision of sea surface height (or slope) determination as possible. The DD altimeter has the potential with respect to measurement precision and spatial resolution to provide a "quantum leap" forward in the mapping of marine gravity and sea floor topography, but the choice of orbit is also a key parameter in the design of the mission. A suggestion for the use of a Near Exact Repeat orbit is made in section 3.5.

The importance of the DD instrument and the mapping of geophysical structures in the 10-20km spatial range for intra basin structures like petroleum exploration is evident. However, sea floor mapping has a great impact for a variety of related oceanographic studies like tide modelling, current modelling, mixing, seafloor tectonics, climate change, tsunami warning etc.

An example of the importance of accurate sea floor mapping is shown in Figure 3-11 from [*Metzger and Hurlburt*, 2001] which shows the Kuroshio mean flow from the U.S. Navy 1/16 degree resolution model. A single uncharted sea-mount with a diameter as small as 20 km dramatically changes the flow pattern.

With the current limitation of altimetric-derived sea floor bathymetry, the size and spatial extent of such a sea mount cannot be charted.

Seamounts with a spatial extent of 20 km and vertical height larger than 2 km are generally charted in existing altimetric maps. However, it is expected that there is still between 40,000 and 50,000 uncharted sea mounts in the world's oceans with height greater than 1 km. These seamounts, which play a key role in a number of oceanographic processes like mixing and tsunami generation / propagation, could be mapped with the observing capabilities of the DD altimeter, if operating from a suitable orbit.

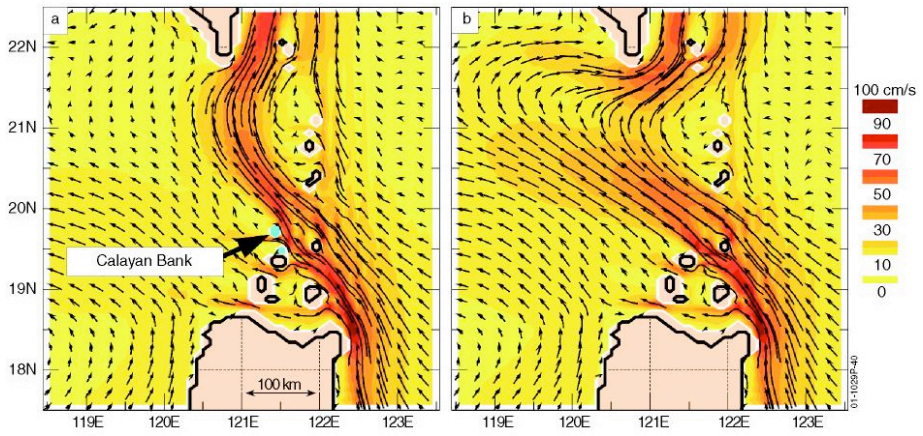

Figure 3-11. The current field across a section of the Kuroshio current showing the importance of accurate sea floor mapping. The figure shows the Kuroshio mean flow from the U.S. Navy 1/16 degree resolution model. Accurate mapping of the Calayan bank sea mount in the figure to the left gives a different flow pattern than the figure to the right, where the Calayan sea mount has been omitted. The Calayan seamount has a spatial extend smaller than 20 km which is the limitation of current satellite altimetry mapping.

3.5.4 Suggested regions for CRYMPS simulations

To allow an investigation into the potential improvement offered by DD altimetry over "conventional" altimetry with respect to the (open ocean) global marine gravity field and sea floor topography mapping, a number of different scenarios are proposed for the CRYOSAT-2 simulation studies planned within this project.

The important parameter for marine gravity and sea floor topography mapping is the variation in sea floor height, hence simulations should be done with sea surface height variations representing geophysical structures of various wavelength and amplitude.

It is expected that an 8 second simulation scenario of 54 km length along track and 8 km across track will be available.

Each scenario will have constant swell amplitude and wavelength which can be varied from simulation to simulation to represent different ocean conditions.

It is suggested to use three scenarios of varying oceanographic conditions here coded **SFT1-3**.

SFT1 swell amplitude = 1 m, wavelength 100m and PDF s.d. = 4 cm

SFT2 swell amplitude = 3 m, wavelength 150m and PDF s.d. = 10 cm

SFT3 swell amplitude = 10 m, wavelength 200m and PDF s.d. = 20 cm

The ocean conditions are equivalent to scenarios F1, F2, and F4 respectively from §3.4.3

It is suggested to use a simulation of two cross-track trenches and two seamounts within the 54 km simulation. The simulation can be carried out modifying the input Digital Terrain Model to the CRYMPS simulation to represent these signals.

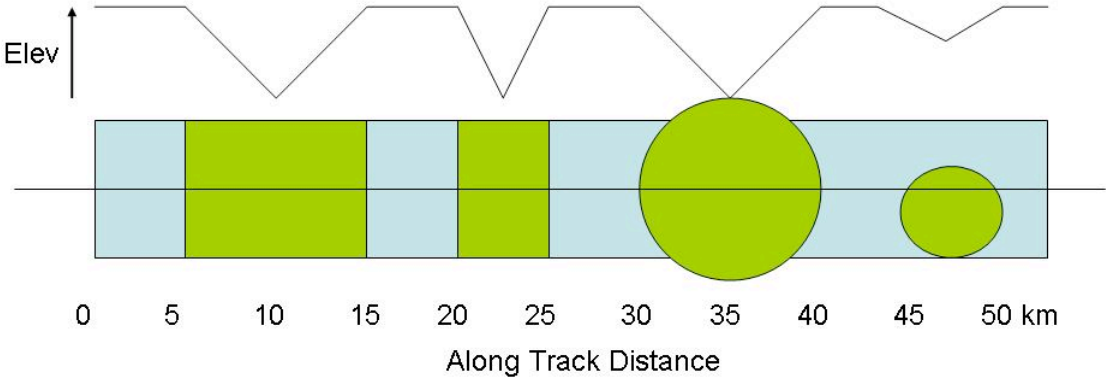

Figure 3-12 – Proposed scenario for CRYMPS simulation to test for sea-floor geophysical information retrieval – what are the slopes of the elevation changes? (state of the art requires slope measurements down to ~ 1 microradian, or a rise of 1mm in a run of 1 km.)

3.5.5 The case for a Near ERM orbit satellite with a DD instrument

For mapping of global marine gravity and sea floor topography the only drawback is the fact that the across-track resolution is not improved and still remains between 2 and 6 km. Similarly the usage of the DD onboard CRYOSAT-2 will be flown in a roughly 320-day repeat orbit which will give an 8 km average track-to-track spacing (at the equator). This orbit configuration is chosen for optimum mapping of the cryosphere and ice-sheets where the interferometric capabilities of the instrument provides uniform along-track and across-track coverage with this configuration.

However, the same cryospheric observations could be obtained if the instrument is launched in a near-exact repeat mission, hereinafter called N-ERM.

In a N-ERM orbit, the spacecraft is allowed a constant drift of between 0 and 10 km in longitude for each repeat (exactly as was done for ERS-1 during its GM). This way the ground tracks will not be repeated, but the earth will gradually be covered with denser and denser ground tracks (4 km after 2 years, 2 km after 4 years, 1 km after 8 years). It is important to note here that a N-ERM orbit has a subsidiary “pseudo-repeat” cycle, after which the orbits are relatively close, although not exactly repeating.

A N-ERM would seem to offer the best option if it is desired to satisfy the needs of cryospheric science, geodesy/geophysical science and oceanographic science in one mission. For oceanography the analysis of these near-repeated observations will only be slightly more complicated than for an exact repeat mission, and with the availability of high quality mean sea surfaces (like DNSC07MSS) and geoid models, only a minor degradation in the results should follow. Thus data from such orbits can be used to support mesoscale oceanographic applications as well as geodesy and other non-repeat orbit applications.

It is evident that the choice of orbit is basically as important as the choice of instrument. The improvement and limitations with the chosen orbit for CRYOSAT-2 will be investigated as a supplementary investigation in WP3 with respect to global marine gravity and sea floor topography mapping using a DD altimeter.

More accurate mapping of the global marine gravity field and sea floor is vital to a number of applications like petroleum exploration, tide modelling, current modelling, mixing, seafloor tectonics, tsunami warning etc. As mentioned, particularly, the off-shore exploration industry would like to have altimeter data with as much resolution as possible and extending as near-shore as possible as most sedimentary basins lie close to the shore.

4 OBSERVING CAPABILITIES OF SAR MODE ALTIMETERS OVER COASTAL OCEAN

4.1 Beneficial aspects of SAR altimetry over coastal ocean

Application of conventional altimetry over coastal regions has been limited, because intrinsic difficulties in the corrections and issues of land contamination in the footprint have so far resulted in systematic flagging and rejection of the data (see *Vignudelli et al*., [2005]). Moreover the conventional along-track resolution (always > 2km even when higher-rate data are used) is insufficient to sample all but the largest scales involved in coastal processes.

The advantageous aspects of SAR altimetry described in Section 3.1 are obviously valid over the coastal ocean as well. One particularly useful advantage in the coastal environment is the reduced (and independent of SWH) footprint along-track length. This allows the resolution of phenomena at spatial scales starting at ~300m. These data would be invaluable for studies of coastal circulation, sea level change and impact on the coastline. In addition, they provide an essential link between the land-based geodetic measurements and oceanic mean sea surface information.

All these features can be usefully exploited for a dramatic improvement of the observing capabilities over the coastal ocean. New and improved applications can take advantage either of the enhanced along-track resolution, or of the enhanced precision, as well as of any desired trade-off amongst those two characteristics. However we must note that whatever improvements we get from SAR altimetry, SSH accuracy still may be limited by the spatial resolution and accuracy of the various necessary corrections (e.g. wet/dry tropospheric correction, etc.).

In the following we list the phenomena that can be observed in the coastal ocean.

4.2 Observable phenomena in the coastal ocean

4.2.1 Sea Level and Tides

It is well known that large-scale tidal models such as the global models used for correcting conventional altimetry records do not reproduce well the signal in proximity of the coast. This results in systematic alias of the residual tidal signal. Coastal SAR altimetry is expected to provide a wealth of information for the improvement in the parameterization of the tidal signal in regional and local tidal models. The resulting de-tided sea surface elevations should be of great interest for assessing that part of the coastal circulation not due to tides.

Long-term sea level change is another item of strategic interest due to its prominent socioeconomic impact, and its rate may vary sharply in space along the coast. The ability of SAR altimetry to recover a good signal in the vicinity of the shore should provide a much more accurate characterization of the local values and trends of sea level.

4.2.2 Waves and coastal set-up

The coastal wave field is a key parameter for any study on coastal dynamics and erosion, imposes precise limits to any operation (like fishing or shipping) in the coastal area and constitutes a major design constraint for any structure at sea. SAR altimetry promises to deliver a measurement of the significant wave height much closer to the coast and therefore invaluable to assess the local conditions and to improve wave models. There should be also room for improving the observations and understanding of coastal setup, as attempted by [*Crout* 1998].

4.2.3 Slicks and Spills

Natural and man-made slicks are an important phenomenon in coastal waters where they have significant effects on the ecosystem and on water quality. The high resolution afforded by SAR altimetry will help detect rapid small-scale variations of σ^0 that can be attributed to slicks, and especially when used in synergy with SAR, marine radar and visible/IR sensors can significantly contribute to assess the frequency and extent of such phenomena. As an example, several areas affected by surface slicks, mostly in form of narrow filaments, are visible in Figure 4-1.

4.2.4 Winds and wind-induced phenomena

A number of small-scale (order of km) wind-related features in the sea surface roughness should be visible in the σ^0 derived-field, these include katabatic winds and sheltering effects (figure 4-1 shows a relevant example), land breeze and island wakes.

At a slightly larger scale, the combination of the wind field and sea level measurements can help identify areas of localized coastal up-welling that hold a great importance for the marine biota.

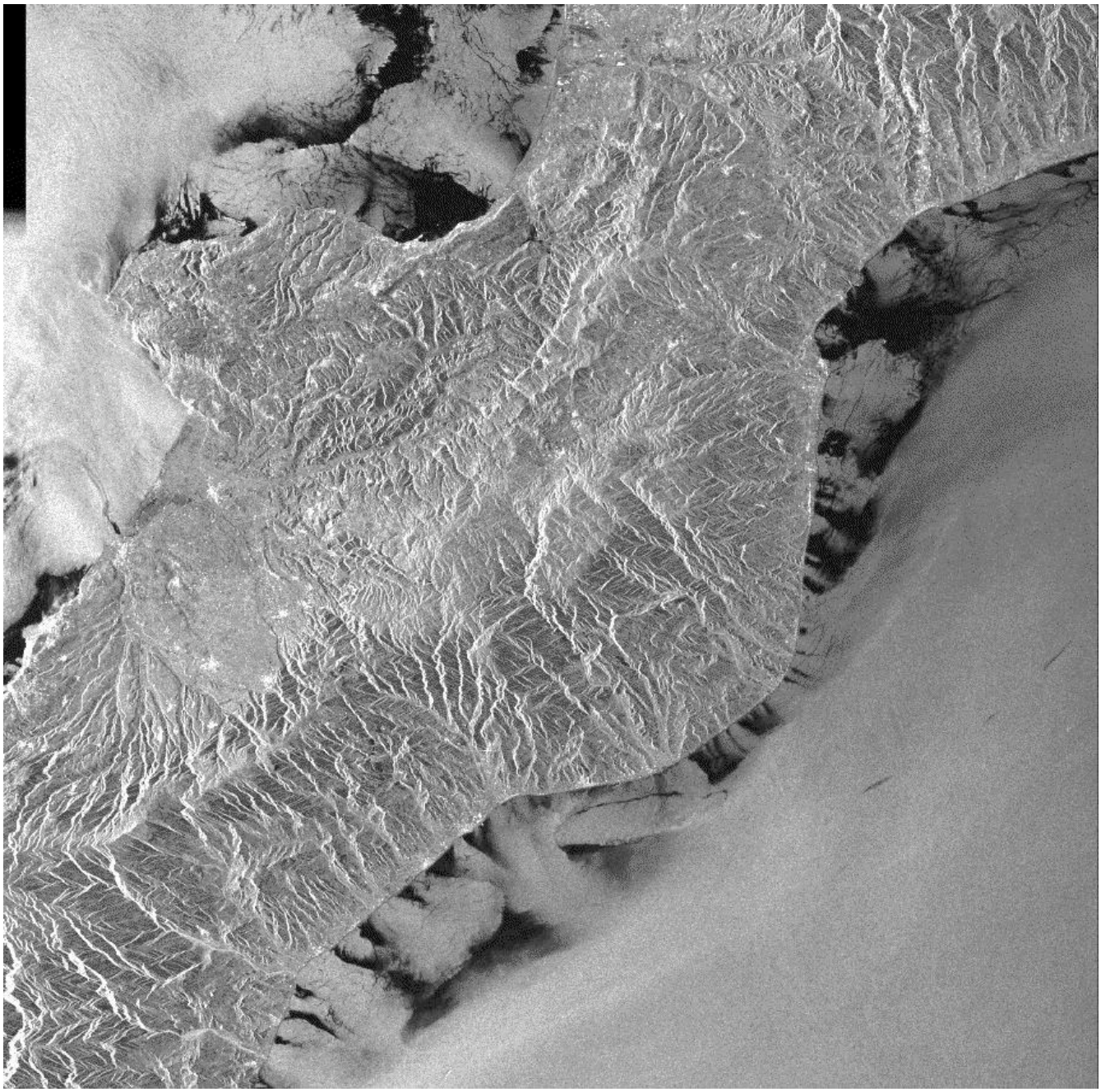

Figure 4-1. ERS-1 SAR image around the region of Calabria in the Mediterranean Sea taken on 22 April 1993 at 21:10. This image shows the σ^0 signature of several katabatic wind events along the coasts (note how closely correlated to land topography they are), and associated sheltering effects, as well as the signature of surface films and slicks [from *Alpers et al.*, 1999]

4.3 CRYMPS simulation scenarios for the coastal ocean

The CRYMPS simulation scenarios for the coastal ocean described in this sub-section have been designed to investigate the detectability of the various phenomena described above in parallel to those proposed for the open ocean in Section 3.4.2. However, one important issue in the coastal environment that differentiates it from the open ocean is the presence of altimeter returns from land. In the SAR altimetry concept, it is in principle possible to maintain range-gate lock on the zero-Doppler return even in presence of strong reflections from land in some of the other Doppler bins [*Raney*, 2005]; therefore it is possible conceptually to do some kind of 'smart processing' that discards the land-affected bins and recovers the useful signal from the sea surface. [*Raney*, 2005] gives as practical lower bound (on how close to the coast the estimation is possible) 500 m for a normal approach to/recession from the shoreline, and approximately 1 km if the track is parallel to the coast.

Following the considerations illustrated above, we have made some modifications to the scenario design criteria, with respect to that done for the open-ocean case in Section 3.4.2:

- the scenarios can now have changing wave/swell parameter, to simulate steepening and shortening of waves

- each scenario can have changing parameters with respect to the scattering surface, at very short scales (1-2 km).

- scenarios can contain land elements. Land elements are regions of high variability for height, polar angle and backscatter (to simulate land it is necessary to generate a specific DEM as input to CRYMPS)

- Ideally we should need to account for changes in wave amplitude and wavelength (and therefore wave slope) when approaching land in shallow bottom. This to some extent can be simulated in the DEM (it may be necessary to reduce the DEM grid spacing to, say 10 or 5 m), and will have to be fine-tuned at a later stage.

Scenarios are still on a standard 8 s duration, corresponding to ~54 km along-track. The three basic ones, 'Normal' (code CN), 'oblique' (code CO) and 'parallel/islands' (code CI) are illustrated in Figure 4-2. Each of them is simulated for each of the following conditions:

CN1/CO1/CI1 SWH = 1m ⇒ swell amp. = 0.71 m, wavelength = 25m and PDF s.d. = 4cm;

CN2/CO2/CI2 SWH = 1m ⇒ swell amp. = 0.71 m, wavelength = 66m and PDF s.d. = 4cm;

CN3/CO3/CI3 SWH = 3m ⇒ swell amp. = 2.12 m, wavelength = 127m and PDF s.d. = 10cm;

CN4/CO4/CI4 SWH = 10m ⇒ swell amp. = 7.07 m, wavelength = 207m and PDF s.d. = 20cm;

where amplitude and wavelength are those for the open ocean, which are then modified locally by approaching the coast. This makes 4 x 3 = **12 simulations in total, codenamed CN1 to CN4, CO1 to CO4 and CI1 to CI4.**

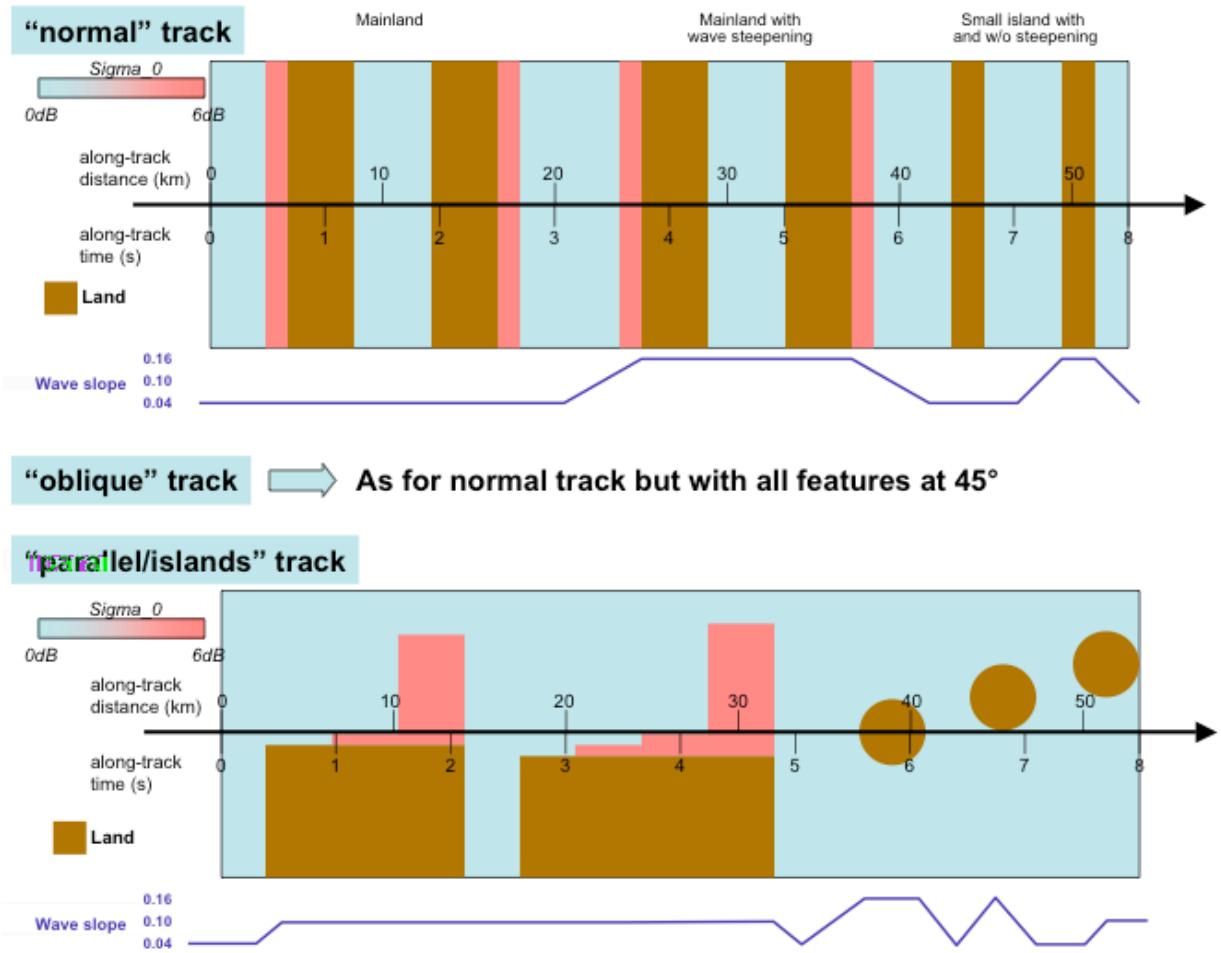

Figure 4-2. Schematic of the three basic scenarios for CRYMPS simulations over the coastal ocean.

5 OBSERVING CAPABILITIES OF SAR MODE ALTIMERS OVER INLAND WATER - REVIEW OF PRIOR WORK

Studies relevant to CryoSat have, naturally, concentrated on ice and, to a lesser extent, ocean surfaces. Accordingly, whilst there is some early work [*Rapley* et al., 1990], [*Guzkowska et al*., 1990] on the possibilities of interferometric altimeter techniques over land surfaces, almost all subsequent research has concentrated on the cryosphere. It is possible that the simulations over sea-ice may have some relevance to the retrieval of inland water information: however, analysis of the Burst Echo data from EnviSat shows extremely complex patterns of quasi-specular and diffuse components returned from inland water [*Berry, et al*., 2007a], [*Berry, et al*., 2007b], a considerably more complex information content than that generally apparent from sea-ice. For illustration, two burst echo sequences, each spanning 10 cycles, are included here. Figure 5-1 shows 10 cycles of data over the Hudson Bay; here, the freeze-thaw cycle is very clearly seen, with one quasi-specular signal dominating during the winter months. Figure 5-2 shows one year of burst echoes obtained over the Congo river system, illustrating very clearly the more complex echo shapes typically returned from inland water. This is likely to prove a significant constraint on applying prior simulations to inland water. This leaves one relevant initiative: the proposed Ka band interferometric altimeter for recovery of inland water heights [*Aldsorf et al.,* 2007]. A brief summary of the concept is given here: more detail, and references to published reports and papers, can be obtained from the WATER-HM website [*Alsdorf et al*., 2008].

The WATER-HM instrument is a near-nadir viewing swath based instrument (with 100km wide swaths) that uses two Ka-band synthetic aperture radar (SAR) antennae at opposite ends of a 10 m boom coupled to a nadir SAR to measure the highly reflective water surface. Interferometric SAR processing of the returned pulses yields a claimed 5m azimuth and 10m to 70m range resolution, with elevation accuracy of ± 50 cm [*Alsdorf et al.*, 2008]. The Ka-band Radar Interferometer (KaRIN) has two 50 km swaths on either side of the nadir track. KaRIN measures the interferometric phase which, together with the system timing measurements, can be turned into an estimate of topography. KaRIN produces simultaneously co-registered images which can be used to delineate water bodies with a spatial resolution which varies continuously from 70 m x 5 m (near swath) to 10 m x 5 m (far swath). The nadir gap is filled by the Ka-band nadir altimeter (AltiKa), which is also used for system calibration. The two instruments are flown in a Prima bus (Alenia) with a 6am-6pm sun-synchronous orbit which optimizes power consumption and spacecraft stability.

The instrument is designed to provide hydraulics measurements of surface water elevations and their derivatives (*dh/dx* and *dh/dt*). Information is summarized below:

- Resolution = 100 m
- Height accuracy = 1 cm / km
- Ka-band SAR interferometric system with 2 swaths, 50 km each
- 200 MHz bandwidth (0.75 cm range resolution)
- Use near-nadir returns for SAR altimeter/angle of arrival mode (e.g. Cryosat SIRAL mode) to fill swath
- No data compression onboard: data downlinked to NOAA Ka-band ground stations

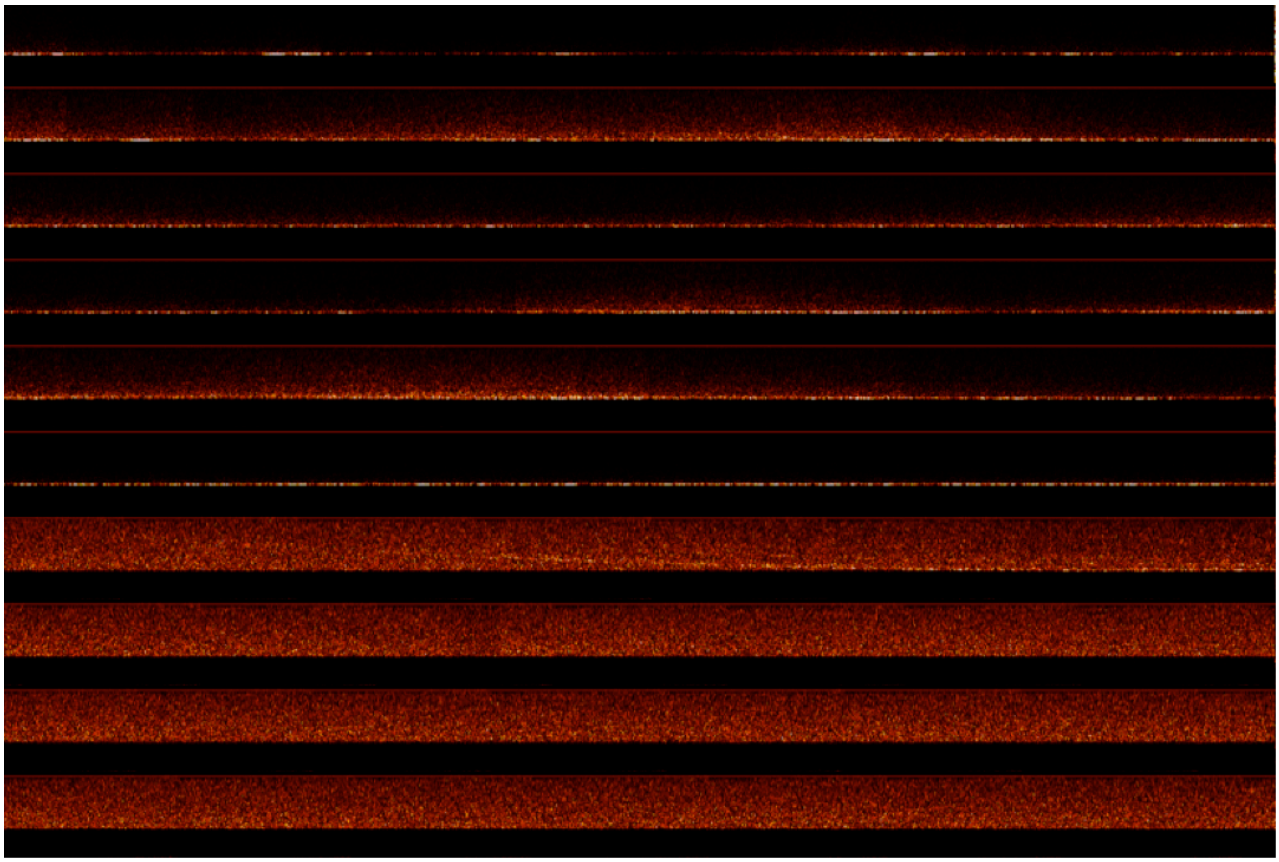

Figure 5-1: Hudson Bay burst echoes (top cycle 33/Dec 04, bottom cycle 42/Nov 05)

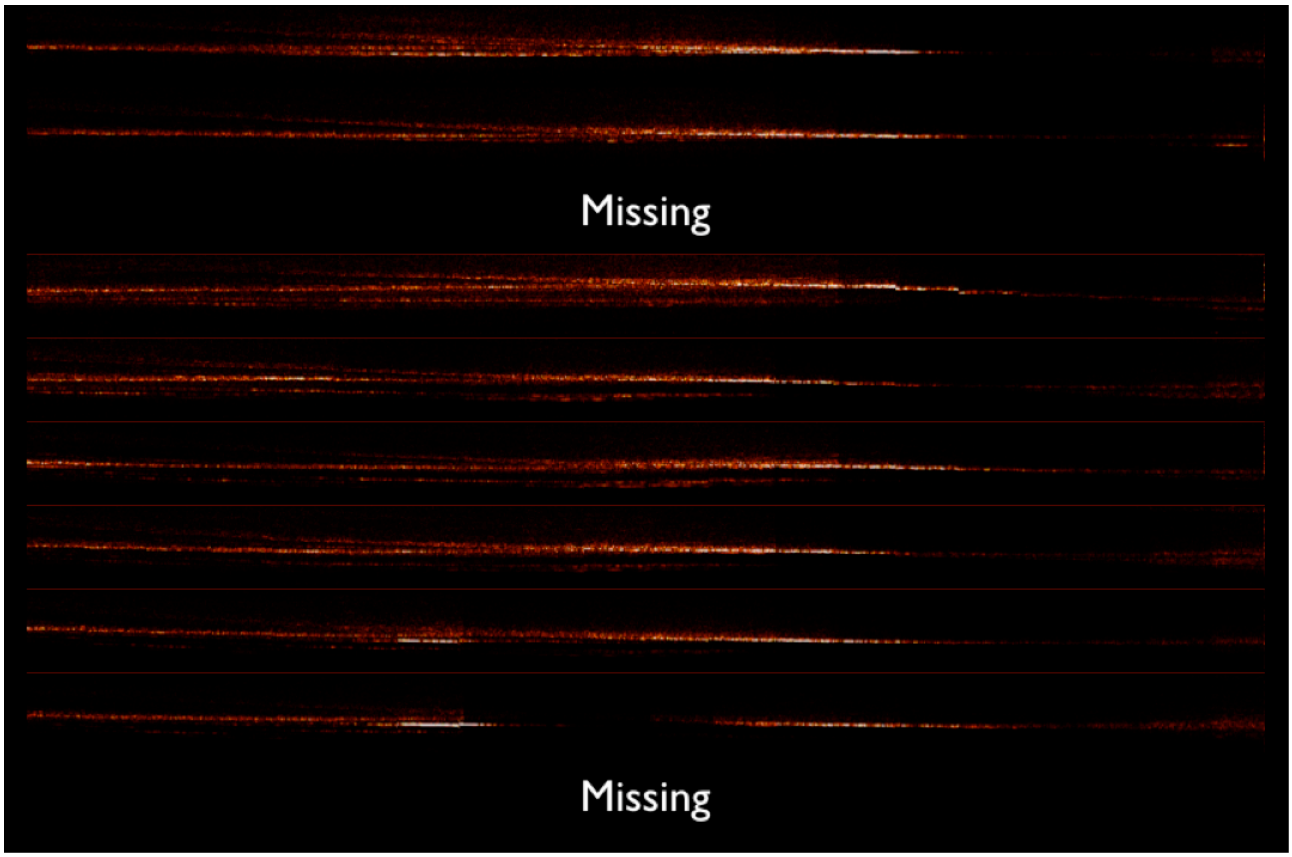

Figure 5-2: Congo River burst echoes (top cycle 33/Dec 04, bottom cycle 42/Nov 05)

The choice of Ka band was dictated by the stringent accuracy and resolution requirements imposed on this mission by its goal of measuring both height and flow rate on moderate sized rivers. However, one already identified constraint on this mission is the significant loss of power caused by signal attenuation through the atmosphere in the presence of heavy precipitation. Since many major river systems are fed by local precipitation, this may impose some limitations on the instrument's measurement capabilities.

Whilst there are a number of publications discussing this mission, the development is at an early stage, and comprehensive search of the available literature has only produced a small number of quantitative simulation studies, with a constrained physical structure. Specifically, the numbers of quasi-specular targets envisaged as within the instrument's view at any time is very small (generally simulations are restricted to two primary targets at any time). Research utilizing the burst echoes from EnviSat has already shown that at Ku band multiple targets are actually seen, with even small pools of water contributing significantly if close to the nadir point. In general, therefore, the status of research supporting this mission is early development, and little useful data are available at this time.

It is therefore concluded that it is probable that the CryoSat-2 altimeter operation over land and inland water will inform the WATER-HM mission design, but the research and simulation studies for the WATER-HM mission are at too early a stage to give realistic information that could be applied to CryoSat-2.

The focus of the land and inland water analysis must therefore be much more targeted towards the CRYMPS simulations and analysis of existing altimeter data rather than drawing on pre-existing published research.

5.1 CRYMPS simulation scenarios for inland waters

A minimum of two scenarios are envisaged to support the studies over inland waters, these will be requested during Phase 2 of the project:

IW1: Amazon Basin (DMU have derived model data for this which needs to be recast in the appropriate inut files and formats).

IW2: Canadian Lakes.

Further scenarios are under consideration.

6 SUMMARY

6.1 Technical Aspects of SAR Altimetry

Through the application of new signal generation and processing techniques, SAR altimetry, or Delay Doppler altimetry, is able to offer a number of benefits in terms of measuring the ocean surface. These include an increase in along track resolution (to ~300m from ~7000m), improved precision in the measurement of the sea surface height (by an estimated factor of two), smoothed “speckle noise”, and a significant improvement in signal to noise ratio (which should result in an improvement in the accuracy of the significant wave height estimate). Section 2 has described how these improvements follow from the Delay Doppler processing, but also shows that a new understanding of the ocean reflected waveform produced by this technique must be developed to better estimate the improvements that are possible. This review has not considered in detail the differences between the waveforms generated by a Delay-Doppler altimeter and those from a conventional altimeter, This is an important aspect, offering potential new applications and measurements, and will be addressed at a later stage in the study.

Thus, the ‘state of the art’ review in Section 2 marks the starting point for proposed theoretical developments in waveform modelling and processing that are necessary to provide a better understanding of the improvements in radar altimeter measurements of the ocean surface that are the focus of this study.

6.2 Measurements over the Open Ocean

Ocean Surface

Section 3 discusses the potential for improved understanding of open ocean phenomena through Delay Doppler altimeter measurements, in terms of improved accuracy and improved along track resolution. The major gains are perhaps to be found in the higher resolution of small-scale oceanic features such as fronts, eddies and slicks, and long period swell. Delay Doppler altimetry may also offer the potential to make measurements of parameters previously not available through conventional altimetry, such as wave skewness. However, the scope of study is effectively limited by the range of input parameters that can be varied in the CRYOSAT altimeter simulator available to the partners, CRYMPS. Thus the scenarios that will be modelled will consider changes in sea surface height, backscatter, wave height and wave length, but the modelling of effects involving a non-Gaussian sea-surface (necessary to investigate wave characteristics such as skewness) is not within the current capabilities of CRYMPS.

Sea Floor Topography

The application of ocean measurements from satellite altimetry has supported a mapping of sea floor topography to a degree previously not possible. However, this technique in turn had its limitations, which were a maximum effective along track resolution of 16 km (this varies with latitude and longitude). The application of delay-Doppler altimetry offers the following benefits:

- Along-track footprint length is constant (does not vary with wave height)
- Factor of 20 improvement in along track resolution (6km to 300m)
- Signal to noise ratio is improved, which should provide more precise sea-surface height measurements.

There remain an estimated 40,000-50,000 unmapped seamounts in the world ocean with heights greater than 1km that could be mapped with the improved resolution and precision of a SAR altimeter in a suitable orbit. The improved mapping of these features could significantly affect the modelling and understanding of ocean dynamics in the regions around them.

6.3 Measurements over the Coastal Ocean

The potential benefits of SAR altimetry in the coastal ocean are even greater than the open ocean, as the typical spatial scales of variability in sea surface height, wave height and period, and sea surface backscatter are much smaller. In addition, once the 6 km along track footprint impinges on land then no ocean measurements could be retrieved. Thus a SAR mode altimeter offers the potential of significant improvements in the critical coastal region. These data would be invaluable for studies of coastal circulation, sea level change and impact on the coastline. In addition, they provide an essential link between the land-based geodetic measurements and oceanic mean sea surface information.

New and improved applications can take advantage either of the enhanced along-track resolution, or of the enhanced precision, as well as of any desired trade-off amongst those two characteristics. However we must note that whatever improvements we get from SAR altimetry, they may be limited by the spatial resolution and accuracy of the various necessary corrections (e.g. wet/dry tropospheric correction, etc.).

Relevant phenomena include:

- Sea level and tides
- Waves and coastal set-up
- Slicks and spills
- Winds and wind induced phenomena

6.4 Measurements over Inland Water

The research and simulation studies for the WATER-HM mission are at too early a stage to give realistic information that could be applied to CryoSat-2. Indeed it is probable that the CryoSat-2 altimeter operation over land and inland water will inform the WATER-HM mission design. The focus of the land and inland water analysis must therefore be much more targeted towards the CRYMPS simulations and analysis of existing altimeter data rather than drawing on pre-existing published research.

6.5 CRYMPS Simulation Scenario Summaries:

The strategy for the ordering and running of CRYMPS simulations is to initially run a first batch of scenarios (see §3.4.3) over some simple idealized scenarios F1-F6, plus the C1-C3 scenarios (from the inversion of a wave spectrum) and the SFT1-SFT3 scenarios (see §3.5.4) to model the effect of a change in sea surface height, as would be induced by variability in sea-floor topography. Then, after some analysis of the output from these initial runs, we plan to run some follow-on more complex scenarios to investigate potential improvements in ocean surface measurements offered by SAR altimetry over the open ocean. Also, at least 2 scenarios will be required over inland waters. We have initially designed six runs with fixed wave height and wavelength conditions over two tracks with varying backscatter features of different geometries, representing “frontal” features (coded OF1-6), and “cell-like” features (coded OC1-6).

For the coastal ocean 3 sets of runs under 4 sea state conditions are proposed to simulate the altimeter track crossing land normal to the track (coded CN1-4), crossing land at an oblique angle to the track (CO1-4), and altimeter crossing discrete islands, and land parallel to the ground track (CI1-4). The effects of wave steepening near the coast are also included. All scenarios are summarized in the following tables:

SAMOSA CRYMPS RUNS – SUMMARY TABLES

FIRST BATCH RUNS

F runs: idealized runs with double purpose a) familiarize with CRYMPS output and b) test different single-component scenarios (F1-F4) or instrument step/impulse response (F5-F6)

C runs: runs with a realistic wave spectrum on which WP2 science is based

SFT runs: Sea Floor Topography runs on which WP3 science is based

As many as possible of these in the first batch (10 in total) now need to be run at a steady pace to allow the project to proceed swiftly to the science phase. They are listed in order of priority with the expected date of delivery based on information by MSSL (they expect to be able to run two scenarios in parallel and provide two full runs every two weeks).

Code	Description	SWH	Swell Ampl.	lambda	PDF s.d.	DEM by	Ref. Fig.	Expected date of delivery
Merged F1/F3	F1: Initial simple scenario with moderate sea conditions (corresponds to CRYOVEX 2006 conditions, 02/05/2006)	1.41m	1.0 m	100 m	4 cm	**MSSL**	3-6	Delivered 25/1
	F3: Initial simple scenario with low sea conditions (corresponds to CRYOVEX 2006 conditions, 30/04/2006)	0.71m	0.5 m	50 m	4 cm			
Merged F2/F4	F2: Initial simple scenario with moderate to high sea conditions	4.23 m	3.0 m	150 m	10 cm	**MSSL**	3-6	Delivered 25/1
	F4: Initial simple scenario with high sea conditions	14.1 m	10 m	200 m	10 cm			
C3	Realistic mono-directional (along-track) wave spectrum, variable along-track	1/2/3 m		Elfouhaly spectrum	10 cm	**NOCS**		Delivered 5/2
SFT1	Sea Floor Topography 1, variations in sea surface height, low swh, short wavelength	1.41 m	1.0 m	100 m	4 cm	**MSSL or DNSC**	3-12	Started 07/2
C1	Realistic omni-directional wave spectrum, variable along-track	0.1/1/2 m		Elfouhaly spectrum	10 cm	**NOCS**		22/2
SFT2	Sea Floor Topography 2, variations in sea surface height, moderate swh and wavelength	4.23 m	3.0 m	150 m	10 cm	**MSSL or DNSC**	3-12	22/2
C2	Realistic omni-directional wave spectrum, variable along-track	2/3/4 m		Elfouhaly spectrum	10 cm	**NOCS**		7/3
SFT3	Sea Floor Topography 3, variations in sea surface height, low swh, short wavelength	14.1 m	10.0 m	200 m	20 cm	**MSSL or DNSC**	3-12	7/3
F5	F1 over varying $\sigma 0$ surface	1.41 m	1.0 m	100 m	4 cm	**MSSL**	3-4	21/3
F6	F1 over varying SSH surface	1.41 m	1.0 m	100 m	4 cm	**MSSL**	3-4	21/3

FOLLOW-ON RUNS

This 'matrix' includes runs for the coastal ocean as defined in section 4.3 of the WP1 report, and runs for inland waters as outlined in Section 5. They would be **26 runs in total** but we will not want to run them all: once the analysis of the data from the first batch can start, we should be able to cherry-pick (or merge) some of them so that the number of CRYMPS runs is kept to a minimum.

Code	Description	SWH	Swell Ampl.	lambda	PDF s.d.	DEM by	Ref. Fig.
OF1 / OC1	Ocean Fronts 1 / Ocean Cells 1: low swh, short wavelength	1.0 m	0.71 m	25 m	4 cm	**NOCS**	3-5
OF2 / OC2	Ocean Fronts 2 / Ocean Cells 2: low swh, medium wavelength	1.0 m	0.71 m	66 m	4 cm	**NOCS**	3-5
OF3 / OC3	Ocean Fronts 3 / Ocean Cells 3: moderate swh, short wavelength	3.0 m	2.12 m	66 m	10 cm	**NOCS**	3-5
OF4 / OC4	Ocean Fronts 4 / Ocean Cells 4: moderate swh, medium wavelength	3.0 m	2.12 m	127 m	10 cm	**NOCS**	3-5
OF5 / OC5	Ocean Fronts 5 / Ocean Cells 5: moderate swh, long wavelength	3.0 m	2.12 m	207 m	10 cm	**NOCS**	3-5
OF6 / OC6	Ocean Fronts 6 / Ocean Cells 6: high swh, long wavelength	10 m	7.07 m	207 m	20 cm	**NOCS**	3-5
CN1/ CO1/ CI1	Normal land / oblique land-sea boundary / islands and parallel coastline: low swh, short wavelength	1.0 m	0.71 m	25 m	4 cm	**NOCS**	4-2
CN2/ CO2/ CI2	Normal land / oblique land-sea boundary / islands and parallel coastline: low swh, medium wavelength	1.0 m	0.71 m	66 m	4 cm	**NOCS**	4-2
CN3/ CO3/ CI3	Normal land / oblique land-sea boundary / islands and parallel coastline: moderate swh, medium wavelength	3.0 m	2.12 m	127 m	10 cm	**NOCS**	4-2
CN4/ CO4/ CI4	Normal land / oblique land-sea boundary / islands and parallel coastline: high swh, long wavelength	10 m	7.07 m	207 m	20 cm	**NOCS**	4-2
IW1	Amazon Basin					**DMU**	
IW2	Canadian Lakes					**DMU**	

7 REFERENCES

Alpers et al. (1999) "The tropical and subtropical ocean viewed by ERS SAR", http://www.ifm.uni-hamburg.de/~ers-sar/,

Alsdorf, D., Fu, L.-L., Mognard, N., Cazenave, A., Rodriguez, E., Chelton, D., and D. Lettenmaier, (2007) Measuring global oceans and terrestrial freshwater from space. *Eos, 88 (24), pp. 253+257.*

Alsdorf, D., Fu, L.L, and N. Mognard, (2008) http://bprc.osu.edu/water/ "The WATER HM Satellite Mission" accessed 02/01/2008

Andersen O. B. and P. Knudsen, (1998) Global Marine Gravity Field from the ERS-1 and GEOSAT Geodetic Mission Altimetry, J. *Geophys. Res., 103(C4), 8129-8137.*

Andersen, O., P. Knudsen and R. Trimmer, (2005) Improved High Resolution Altimetric Gravity Field Mapping (KMS2002 Global Marine Gravity Field), *In F. Sanso (Ed) A window on the Future of Geodesy, IAG symposium, 128, 326-331, Springer Verlag, Heidelberg, Germany.*

Barbarossa, S., and G. Picardi, (1990) "The synthetic aperture concept applied to altimetry: Surface and sub-surface imaging", *Proceedings of the consultative meeting on imaging altimeter requirements and techniques, C.G.Rapley, H.D. Griffiths and P.A.M. Berry, Eds., 30 May - 1 June 1990, Dorking, UK., Mullard Space Science Laboratory Report MSSL/RSG 90.01.*

Berry, P.A.M., Freeman, J.A., Rogers, C., and J. Benveniste, (2007a) Global analysis of Envisat RA-2 burst mode echo sequences. *IEEE Geoscience and Remote Sensing, Volume 45, Issue 9, Pages 2869-2874 DOI: 10.1109/TGRS.2007.902280.*

Berry, P.A.M.; Freeman, J.A.; Rogers, C.; and J. Benveniste, (2007b) Global Analysis of the Envisat RA-2 Burst Echoes *"Envisat Symposium 2007", ESA Pub. SP-636 2007*

Brown, G.S., (1977) " The Average Impulse Response of a Rough Surface and Its Applications" *IEEE Trans. Antennas Propag., vol. AP-25, pp. 67-74, Jan.1977.*

Caputi, W. J. J.(1971) "Stretch: a time-transformation technique," *IEEE Transactions on Aerospace and Electronic Systems, vol. AES-7, pp. 269-278.*

Chelton D.B. (2001) "Report of the high-resolution ocean topography science working group meeting," *Ref. 2001-4. Oregon State University, Corvallis, OR*

Chelton, D. B., E.J. Walsh, and J.L. MacArthur, (1989) "Pulse Compression and Sea Level Tracking in Satellite Altimetry" *J. Atmos. Oceanic Technol., vol. 6, pp. 407-437, June 1989.*

Chelton, D. B. and M. G. Schlax, (1996) "Global observations of oceanic Rossby waves", *Science, 272, 234-238.*

Chelton, D. B., M. G. Schlax, R. M. Samelson and R. A. de Szoeke, (2007) "Global observations of large ocean eddies*". Geophys. Res. Lett., 2007, 34, L15606, doi:10.1029/2007GL030812.*

Cipollini, P., P. G. Challenor, D. Cromwell G. D. Quartly and I. S. Robinson, (2006) "How satellites have improved our knowledge of extratropical planetary waves in the ocean", *ESA SP-614, Proceedings of the Symposium on "15 years of progress in radar altimetry", Venice Lido (Italy), 13-16 March 2006.*

Cotton D., et al, (2004) "GAMBLE - Global Altimeter Measurements By Leading Europeans Requirements for Future Satellite Altimetry: Recommendations for Missions and Research Programmes", *Final Report, 2004*

Crout, R. L. (1998) "Coastal currents from satellite altimetry", *Sea Technology, 8, 33-37.*

Cumming, I.G., and F.H. Wong, (2005) "Digital Processing Of Synthetic Aperture Radar data: Algorithms and Implementation*". Artech House Publishers, ISBN-10: 1580530583, Jan. 2005.*

Cutrona, L.J. , W.E. Vivian, E.N. Leith, and G.O. Hall, (1962) "A high resolution radar combat surveillance system", *IRE Trans. On Military Electronics, vol. MIL-6, pp. 119-133,.*

Elfouhaily, T., B. Chapron, K. Katsaros, and D. Vandemark, (1997) A unified directional spectrum for long and short wind-driven waves,º *J. Geophys. Res., vol. 102, no. C7, pp. 781-796, 1997*

Francis, C.R., (2002) "Design of the CryoSat system", *Proc. IEEE IGARSS 2002, pp1759-1761.*

Francis, C.R., (2007) "Jason Follow-on and CryoSat", *ESA report C2-RP-ESA-SY-0035, September 2007Fu, L-L. , A.Cazenave, "Satellite Altimetry and Earth Science", Academic Press, International Geophysics Series, vol.69, ISBN-0-12-269454-3.*

Fu, L-L. , and A. Cazenave, (2001) "Satellite Altimetry and Earth Science", *Academic Press, International Geophysics Series, vol.69, ISBN- 0-12-269454-3.*

Gomez-Enri et al., (2007) "Measuring Ocean Global Wave-Skewness using Envisat RA-2 Ocean Waveforms", *Proc. Envisat Symposium, Montreux, 2007*

Guymer, T.H., G.D. Quartly, and M.A. Srokosz (1995) "The Effects of Rain on ERS-1 Radar Altimeter Data". *J. Atmos. Oceanic Technol., 12, 1229–1247.*

Guzkowska, M.A.J., Rapley, C.G., Ridley, J.K., Cudlip, W., Birkett, C.M. and Scott, R.F., (1990) "Developments in Inland Water and Land Altimetry", *ESA CR-7839/88/F/FL.*

Hartl, P. Y.H. Kim, (1990) "Multi-mode scanning radar altimeter (MSRA) with synthyetic aperture", Proceedings of the consultative meeting on imaging altimeter requirements and techniques*, C.G.Rapley, H.D. Griffiths and P.A.M. Berry, Eds., 30 May - 1 June 1990, Dorking, UK., Mullard Space Science Laboratory Report MSSL/RSG 90.01.*

Hayne, G.S. (1980), "Radar Altimeter Mean Return Waveform from Near-Normal-Incidence Ocean Surface Scattering" *IEEE Trans. Antennas Propag., vol. AP-28, pp. 687-692, Sep. 1980*

Jensen J. R, and R.K. Raney (1998) "Delay/Doppler Radar Altimeter: Better Measurement Precision", *Proc. IEEE IGARSS 1998, pp. 2011-2013,.*

Kaula, W.M. (1969) "The terrestrial environment: Solid earth and ocean physics", *NASA report study at Williamstown, Mass. Technical Report NASA CR-1579, Aug. 1969.*

MacArthur, J. L., P. C. Marth, and J. G. Wall, (1987) "The GEOSAT Radar Altimeter," *Johns Hopkins APL Technical Digest, vol. 8, pp. 176-181.*

Mackay E., Retzler, C., Challenor, P. & Gommenginger C., (2008) "An Empirical Algorithm for Ocean Wave Period from Ku-band Altimeter Data*. J. Geophys. Research, in press*

Metzger, E. J., Hurlburt, H E, (2001). The Nondeterministic Nature of Kuroshio Penetration and Eddy Shedding in the South China Sea*. Journal of Physical Oceanography, 31: 1712-1732.*

Phalippou, L., and V. Enjolras (2007) "Re-Tracking of SAR Altimeter Ocean Power-Waveforms and Related Accuracies of the Retrieved Sea Surface Height, Significant Wave Height and Wind Speed, *Proc. IEEE IGARSS 2007.*

Peebles, P., Jr., (1998) Radar Principles*, John Wiley & Sons, Inc.*

Quartly, G.D., (1998) "Determination of Oceanic Rain Rate and Rain Cell Structure from Altimeter Waveform Data". Part I: Theory. *J. Atmos. Oceanic Technol., 15, 1361–1378.*

Raney, R. K. , (1994) "Precision SAR Processing Using Chirp Scaling" *IEEE Trans. Geosci. Remote Sensing, vol. 32, pp. 786-799, Jul. 1994.*

Raney, R. K., (1998) "The Delay/Doppler Radar Altimeter" *IEEE Trans. Geosci. Remote Sensing, vol. 36, pp. 1578-1588, Sept.1998.*

Raney, R. K. , (2005) "Resolution and Precision of a Delay-Doppler Radar Altimeter", *Proc. IEEE OCEANS 2005*

Raney, R. K. and J. R. Jensen, (2000) "D2P project: Test campaign results" http://fermi.jhuapl.edu/d2p/, *June 2000.*

Raney, R. K. and D. L. Porter, (2000) "WITTEX: An innovative three-satellite radar altimeter concept", *Proceedings of International Geoscience and Remote Sensing IGARSS 2000.*

Raney, R.K., and J. R. Jensen (2001) "Delay/Doppler Phase-Monopulse (D2P) Instrument Incubator Program (IIP) Final Report", *The JHU- Applied Physics Lab. Laurel, Maryland. July 2001.*

Rapley, C.G., Griffiths, H.D., and Berry, P.A.M., (1990), "Proceedings of the Consultative Meeting on Imaging Altimeter Requirements and Techniques", *ESA Reference MSSL/RSG/90.01.*

Robinson, I. S. (2005) "Measuring the Oceans from Space - The Principles and Methods of Satellite Oceanography", *669 p., Springer-Verlag, 2005*

Sandwell D.T., and W.H.F. Smith, (1997) Marine gravity anomaly from Geosat and ERS 1 satellite altimetry*, J. Geophys. Res.,* 102, 10,039--10,054

Sandwell D. T., W. H. F. Smith, and K. R. Raney, (2004) Bathymetry from Space, *Presentation at the IAG symposium, GGSM, Porto, 2004,*

Sauvageot, H., F. Mesnard, and R.S. Tenório, (1999) "The Relation between the Area-Average Rain Rate and the Rain Cell Size Distribution Parameters". *J. Atmos. Sci., 56, 57–70, 1999*

Smith, W. H. F., (2004) Bathymetry from Space, *Oceanography, vol 17,1, 2004*

Thompson, K. R., and E. Demirov (2006), "Skewness of sea level variability of the world's oceans", *J. Geophys. Res., 111, C05005, doi:10.1029/2004JC002839.*

Vignudelli, S., P. Cipollini, L. Roblou, F. Lyard, G. P. Gasparini, G. Manzella, and M. Astraldi, (2005) "Improved satellite altimetry in coastal systems: Case study of the Corsica Channel (Mediterranean Sea), *Geophys. Res. Lett., 32, L07608, doi:10.1029/2005GL022602.*